Accepted Manuscript

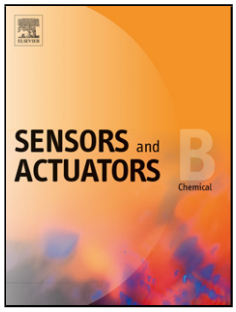

Title: Hybrid Nanoarchitecturing of Hierarchical Zinc Oxide Wool-Ball-Like Nanostructures with Multi-Walled Carbon Nanotubes for Achieving Sensitive and Selective Detection of Sulfur Dioxide

Authors: Ni Luh Wulan Septiani, Yusuf Valentino Kaneti, Brian Yuliarto, Nugraha, Hermawan Kresno Dipojono, Toshiaki Takei, Jungmok You, Yusuke Yamauchi

PII: S0925-4005(18)30088-1
DOI: https://doi.org/10.1016/j.snb.2018.01.088
Reference: SNB 23937

To appear in: *Sensors and Actuators B*

Received date: 14-10-2017
Revised date: 29-11-2017
Accepted date: 5-1-2018

Please cite this article as: Ni Luh Wulan Septiani , Yusuf Valentino Kaneti, Brian Yuliarto, Nugraha, Hermawan Kresno Dipojono, Toshiaki Takei, Jungmok You, Yusuke Yamauchi, Hybrid Nanoarchitecturing of Hierarchical Zinc Oxide Wool-Ball-Like Nanostructures with Multi-Walled Carbon Nanotubes for Achieving Sensitive and Selective Detection of Sulfur Dioxide, Sensors and Actuators B: Chemical https://doi.org/10.1016/j.snb.2018.01.088

This is a PDF file of an unedited manuscript that has been accepted for publication. As a service to our customers we are providing this early version of the manuscript. The manuscript will undergo copyediting, typesetting, and review of the resulting proof before it is published in its final form. Please note that during the production process errors may be discovered which could affect the content, and all legal disclaimers that apply to the journal pertain.

ACCEPTED MANUSCRIPT

Hybrid Nanoarchitecturing of Hierarchical Zinc Oxide Wool-Ball-Like Nanostructures with Multi-Walled Carbon Nanotubes for Achieving Sensitive and Selective Detection of Sulfur Dioxide

Ni Luh Wulan Septiani,[1,2,+] Yusuf Valentino Kaneti[3,*,+] Brian Yuliarto,[1,4,*] Nugraha,[1,4] Hermawan Kresno Dipojono,[4] Toshiaki Takei,[3] Jungmok You,[5] Yusuke Yamauchi[3,5,6,7,*]

[1] Advanced Functional Materials (AFM) Laboratory, Engineering Physics, Institute of Technology Bandung, Bandung 40132, Indonesia.

[2] Welding Engineering Department, Institute of Technology Science Bandung, Cikarang Pusat, Bekasi 17530, Indonesia.

[3] World Premier International (WPI) Research Center for Materials Nanoarchitectonics (MANA), National Institute for Materials Science (NIMS), 1-1 Namiki, Tsukuba, Ibaraki 305-0044, Japan.

[4] Research Center for Nanosciences and Nanotechnology (RCNN), Institute of Technology Bandung, Bandung 40132, Indonesia.

[5] Department of Plant & Environmental New Resources, Kyung Hee University, 1732 Deogyeong-daero, Giheung-gu, Yongin-si, Gyeonggi-do 446-701, South Korea

[6] Australian Institute of Innovative Materials (AIIM), University of Wollongong, North Wollongong, New South Wales 2500, Australia.

[7] School of Chemical Engineering & Australian Institute for Bioengineering and Nanotechnology (AIBN), The University of Queensland, Brisbane, QLD 4072, Australia

[+]These authors contributed equally to this work

Emails: brian@tf.itb.ac.id; KANETI.Valentino@nims.go.jp; Yamauchi.Yusuke@nims.go.jp

ACCEPTED MANUSCRIPT

ACCEPTED MANUSCRIPT

Graphical abstract

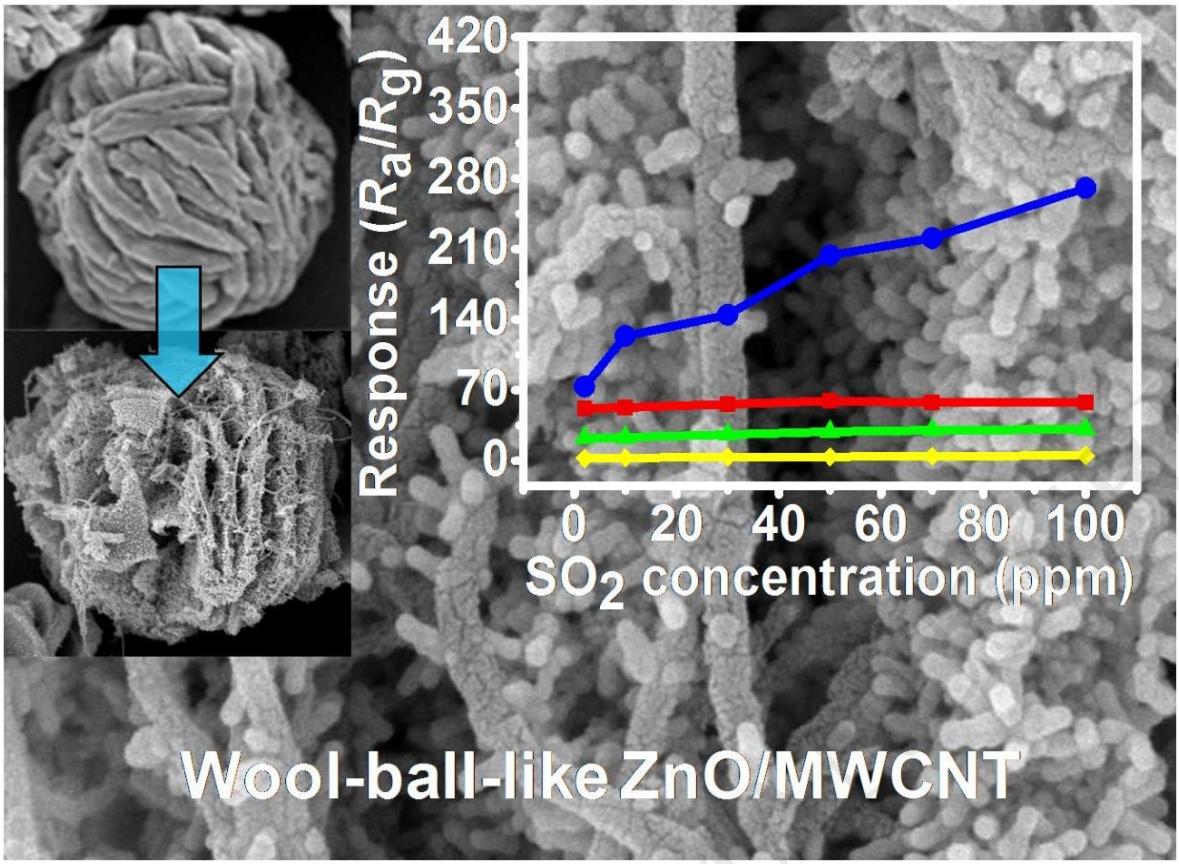

Research highlights

- Hierarchical 3D wool-ball-like ZnO nanostructures were synthesized via a solvothermal method.
- 3D wool-ball like ZnO/MWCNT composites with different ratios (3:1, 5:1, and 10:1) were prepared.
- The 3D wool-ball like ZnO/MWCNT composite showed high response and good selectivity to SO_2 gas.

Abstract

This work reports a facile glycerol-assisted solvothermal method for synthesizing hierarchical three-dimensional (3D) wool-ball-like zinc oxide (ZnO) nanostructures and their subsequent modifications with multi-walled carbon nanotubes (MWCNTs) as modifiers for achieving sensitive and selective detection of toxic sulfur dioxide (SO_2) gas. Structurally, the as-synthesized 3D wool-ball-like ZnO is assembled of two-dimensional (2D) plate-like structures, which

ACCEPTED MANUSCRIPT

themselves are arranged by numerous small nanoparticles. Furthermore, in this work we observed an interesting new phenomenon in which when a high concentration of MWCNTs is introduced, many small nanorods grew on the surface of the plate-like structures which assemble the 3D wool-ball-like ZnO nanostructures. When evaluated for SO_2 detection, the ZnO/MWCNTs (10:1) composite (ZnO:MWCNTs= 10:1) shows a high response of 220.8 to 70 ppm of SO_2 gas (approximately three times higher than the response of pure wool-ball-like ZnO) at an optimum operating temperature of 300 °C. Additionally, the composite also displays good stability and selectivity to SO_2 with the response to 50 ppm of SO_2 being 7-14 times higher than the responses to other tested gases at a similar concentration. The excellent sensing performance of the wool-ball-like ZnO/MWCNTs (10:1) composite is mainly attributed to: (i) the formation of *p-n* heterojunctions at the ZnO/MWCNTs interfaces, which greatly enhances the resistance changes upon exposure to SO_2 gas and (ii) the increased amount of adsorption sites for O_2 and SO_2 gas molecules owing to the larger surface area of the composite and defects sites generated by the functionalization process of MWCNTs.

Keywords: zinc oxide, porous metal oxides, sulfur dioxide sensor, gas-sensing, carbon nanotubes, metal oxide nanocomposites

1. Introduction

In recent years, the development of gas sensors for the environmental monitoring of toxic gases has become an increasingly important issue due to the growing concerns regarding air pollution in the world. Among various noxious gases, sulfur dioxide (SO_2) is one of the most toxic and common air pollutants.[1] SO_2 is generated in the environment mainly from the combustion of sulfur-containing compounds such as coal and fuel oil and natural reactions such as volcanic eruptions and forest fires.[2, 3] Furthermore, it can interact with the water vapor in the atmosphere and becomes converted to sulfuric acid which contributes to the acid rain, which causes acidification of lakes and streams, accelerates corrosion of buildings and reduces visibility.[1] In addition, SO_2 also promotes the formation of microscopic acid aerosols, which have serious health implications as well as contributing to climate change. SO_2 is highly toxic to humans as repeated exposure to low concentrations of SO_2 (<5 ppm) can lead to breathing problems, respiratory illnesses, poorer lung defense, and worsening respiratory and cardiovascular diseases.[1, 2] For humans, the acceptable long-term and short-term exposure limits of SO_2 gas are 2–5 ppm, respectively, however the acceptable limit of SO_2 in ambient air is significantly lower.[3]

ACCEPTED MANUSCRIPT

To date, various sensors have been developed for SO_2 detection including optical,[4] chromatography,[5] conductometric, surface acoustic wave (SAW),[6] and Fourier transform infrared spectrometry.[7] Among these, conductometric sensors based on metal oxide semiconductors (MOS) are the most widely used due to their low cost, high sensitivity, and ease of fabrication and processing.[1] Many MOS such as tin oxide (SnO_2),[8, 9] zinc oxide (ZnO),[10, 11] tungsten oxide (WO_3),[12, 13] and titanium dioxide (TiO_2)[14, 15] have been exploited in conductometric gas sensors. ZnO which possesses a wide band gap 3.3 eV and a high exciton binding energy of ~60 meV is among the most widely investigated MOS for gas sensors, owing to their high thermal and chemical stabilities, low synthesis cost, highly controllable morphology, as well as high sensitivity to many gases.[10] To date, various ZnO nanostructures including 1D (nanorods,[16-18] nanowires,[19] nanotubes[20]), 2D (nanoplates,[21] nanoflakes,[22] nanosheets[23, 24]) and 3D (flower-like,[25, 26] urchin-like[27]) have been reported. Among these, hierarchical 3D ZnO nanostructures have attracted significant interests as they possess both high surface area and porosity, which lead to a high amount of active sites and improved adsorption of gas molecules. To date, 3D ZnO nanostructures have shown high sensitivity to ethanol,[28] NH_3,[29] and acetone.[30] However, the sensitivity of pristine ZnO nanomaterials toward SO_2 gas tend to be relatively low and require further modifications to enhance their practical applicability.[1]

At present, various methods are available for enhancing the gas-sensing performance of metal oxide-based sensors, including surface, interfacial and structural modifications.[16, 31, 32] Surface modifications utilize catalytic reactions which can increase surface reaction rates in order to enhance the sensing response and/or lower the optimum operating temperature of metal oxide-based sensors. Generally, surface modifications rely on the use of catalytically active noble metals such as gold (Au),[33] silver (Ag),[34, 35] platinum (Pt),[36] and palladium (Pd).[37] However, the high cost of noble metals metal made this method rather unfavorable for practical gas sensor applications. Interfacial modifications combine two materials of similar or different types of semiconductors to form *n-n*, *p-p*, or *p-n* heterojunction.[31] In comparison, structural modifications rely on the size reduction or morphological modification of the sensing materials to enhance their specific surface area and therefore, the amount of available active sites for gas adsorption or to expose the most active crystal facets.[16, 22] Carbon nanomaterials such as graphene oxide, single- (SWCNTs) and multi-walled carbon nanotubes (MWCNTs) have been proposed as potential modifiers to metal oxide sensors owing to their large surface area and high electrical conductivity at low temperatures. However, carbon materials such as MWCNTs exhibit strong sp^2 bonds, leading to poor chemical reactivity with most gas molecules and they can react only when exposed to

ACCEPTED MANUSCRIPT

strong oxidizing or reducing gases. As a consequence, bare MWCNTs tend to be insensitive, non-selective, irreversible, and slow in responding and/or recovering.[38] Modifications of MWCNTs with noble metals have been shown to enhance their sensing response to gases such as NH_3,[39] CO, ethanol.[40] However, such methods tend to be expensive and unfavorable for practical applications. Therefore, the modification of MWCNTs with cheaper metal oxides may offer a more promising way of overcoming their limitations for gas-sensing applications.

Herein, we report synthesis of three-dimensional (3D) wool-ball-like ZnO particles assembled by two-dimensional (2D) plate-like sub-units, which themselves are arranged by hexagonal-shaped nanoparticles using a glycerol-assisted solvothermal approach. The effects of reaction time and concentration of glycerol on the formation mechanism of the wool-ball-like ZnO precursor particles were studied. Moreover, to induce interfacial modifications, the wool-ball-like ZnO particles were subsequently modified with MWCNTs at different ratios from 10:1 to 3:1. Interestingly enough, when a high concentration of MWCNTs is introduced, the formation of many small nanorods the surface of the plate-like subunits assembling the 3D wool-ball-like ZnO is observed. To the best of our knowledge, such a unique phenomenon has not been reported in previous literatures related to ZnO. The effect of the amount of MWCNTs on the SO_2 sensing performance of the wool-ball-like ZnO sensor was investigated in terms of sensitivity, selectivity, and stability. Among the three composite sensors, the wool-ball-like ZnO/MWCNTs (10:1) sensor displays the highest sensing response of 220.8 to 70 ppm of SO_2 gas, which is roughly three times that of the pure wool-ball-like ZnO sensor at an optimum operating temperature of 300 °C. The combined use of interfacial and structural modifications demonstrated in this study may assist in future development of highly sensitive and selective sensing materials for the detection of environmentally hazardous gases.

2. Experimental section

2.1 Functionalization of multi-walled carbon nanotubes (MWCNTs)

The procedure for the functionalization of the MWCNTs was similar to a previous report.[41] In a typical process, 300 mg of MWCNTs (Fig. S1a-c, ESI) were dispersed in a mixture of nitric acid (HNO_3) and sulfuric acid (H_2SO_4) with ratio 3:1. The suspension was sonicated at 80 °C for 3 h and subsequently washed and rinsed with distilled water for several times until the pH became neutral. The functionalized MWCNTs were then dried at 80 °C for 16 h and used for further experiments.

ACCEPTED MANUSCRIPT

2.2 Synthesis of hierarchical 3D wool-ball-like ZnO nanostructures

In a typical procedure, 0.5 mmol of $ZnNO_3.6H_2O$ was dissolved in 40 mL of 2-propanol. Next, 8 mL of glycerol was added into the mixture solution and stirred until homogenous mixed. Following this, the mixture solution was transferred into a 100 mL stainless steel-lined Teflon autoclave and heated at 180 ℃ for 16 h. The obtained precipitate was subsequently rinsed with ethanol several times followed by drying at 60 ℃ for 6 h. The dried powder was finally calcined at 350 ℃ for 2 h with heating rate 1 ℃ min^{-1} to obtain the wool ball-like ZnO nanostructures. To investigate the growth mechanism of the wool-ball-like ZnO, additional experiments were carried out using different amount of glycerol (0 ml, 2 ml, 4 ml, 8 ml, and 10 ml) and different reaction time (2 h, 4 h, 8 h, and 16 h).

2.3 Synthesis of hierarchical 3D wool-ball-like ZnO/MWCNTs composites

A certain amount of MWCNTs was dispersed in 40 mL of 2-propanol and sonicated for 1 h. Next, 0.5 mmol of $ZnNO_3.6H_2O$ was added into the suspension and stirred for 30 minutes. Following this, 8 mL of glycerol was added into the solution and stirred for another 30 minutes. After that, the mixture solution was transferred into a 100 mL stainless steel-lined Teflon autoclave and heated at 180 °C for 16 h. The obtained precipitate was then washed with ethanol for several times and dried at 60 °C for whole night. The as-synthesized powder was finally calcined at 350 °C for 2 h with heating rate 1 °C min^{-1} to obtain the wool-ball-like ZnO/MWCNTs nanocomposite. In this study, three different ZnO/MWCNTs composites were prepared using three different ZnO:MWCNTs ratios of 10:1, 5:1, and 3:1 and accordingly, these samples are labeled as ZnO/MWCNTs (10:1), ZnO/MWCNTs (5:1), and ZnO/MWCNTs (3:1) composites.

2.4 Characterization

X-ray diffraction patterns of the samples were obtained with a Rigaku RINT 2500X diffractometer using monochromated Cu-Kα radiation (λ= 1.5418 Å). The morphology and microstructure of the products were examined using the field-emission scanning electron microscope (FESEM) (Hitachi SU-8000) and transmission electron microscope (TEM) (JEOL JEM-2100F). The thermogravimetric analysis (TGA) was performed using a Hitachi HT-Seiko Instrument Exter 6300 TG/DTA under an air atmosphere with a constant heating rate of 10 ℃ min^{-1} from room temperature to 800 ℃. The nitrogen (N_2) adsorption-desorption measurements of the samples were performed using a Belsorp-mini II Sorption System at 77 K. The specific surface areas of the samples were measured using the multipoint Brunauer-

ACCEPTED MANUSCRIPT

Emmett-Teller (BET) method at a relative pressure (P/P_0) range of 0.05 to 0.30. Prior to the BET measurements, all the samples were degassed under vacuum for overnight at 150 °C.

2.5 Sensor fabrication and gas-sensing tests

For the gas-sensing tests, alumina substrates with Ag electrodes were used. To prepare the sensor, a certain amount of the pure ZnO or ZnO/MWCNTs composite powder was dispersed in ethylene glycol to form slurry. The slurry was subsequently deposited onto an alumina substrate using the doctor blade technique. The deposited film was then dried at 200 ˚C for 1 h. The external wire and the gas sensor substrate were connected through a gold needle where one end of the needle was connected to the gas-sensor substrate while the other end was connected to an external wire. The change in resistance of the sensor was measured using Picotest M3500A digital multimeter and recorded by a computer. The temperature of the heater was controlled using the Omron G3PX-220EH instrument. The concentration of SO_2 was controlled by nitrogen mixing and was measured using the Bacharach PCA3 portable gas analyzer. Air compressor was utilized to provide clean air into the chamber. The response of the sensor (S) is defined as $S= R_a/R_g$, where R_a and R_g are the resistances measured in air and target gas, respectively. The schematic illustration and the digital photograph of our gas-sensing measurement system are given in Fig. S2a and b (Supporting Information), respectively. Furthermore, the digital picture of the ZnO/MWCNTs sensor is given in Figure S2c (Supporting Information). During the gas-sensing tests, the change of resistance was measured using the Picotest M3500A digital multimeter. The temperature of the heater was controlled using the Omron G3PX-220EH instrument. The resistance of the sensor was recorded by the computer. Prior to the test, the chamber was purged with highly pure nitrogen (99.9%) until the display showed 0 ppm of SO_2. Once fully purged, SO_2 gas is introduced into the chamber by mixing it with nitrogen gas and its concentration was controlled by tuning the nitrogen concentration in the mixing chamber, as measured using the Bacharach PCA3 portable gas analyzer. Air compressor was utilized to provide clean air into the chamber. The gas-sensing experiments were conducted at a relative humidity of 73-74%. The response of the sensor (S) is defined as $S= R_a/R_g$, where R_a and R_g are the resistances measured in air and target gas, respectively. A schematic illustration of the set-up of the gas-sensing measurement system is given in Fig. S2 (Supporting Information).

3. Results and discussion

3.1 Morphology and composition

ACCEPTED MANUSCRIPT

The XRD pattern of the ZnO precursor sample obtained from the solvothermal reaction between zinc nitrate and glycerol in 2-propanol at 180 °C is shown in Fig. S3 (Supporting Information). The product can be indexed to a mixture of zinc hydroxide ($Zn(OH)_2$) and zinc hydroxide carbonate ($Zn_5(OH)_6(CO_3)_2$).[42, 43] The thermogravimetric curve of this precursor sample reveals two main weight loss steps, with the first weight loss (6.10%) occurring at around 150 °C due to the removal of adsorbed water molecules and the second one (48.9%) occurring from around 300 °C, which is attributed to the decomposition of the zinc hydroxides to form ZnO (Fig. 1a). The complete transformation to ZnO can be achieved at a temperature of ~350 °C. Fig. 1b shows the XRD pattern of the calcined ZnO precursor sample at 350 °C, which reveals the presence of several diffraction peaks indexed to the (100), (002), (101), (102, (110), (103), and (112) planes of hexagonal wurztite ZnO (JCPDS No. 36-1451). No peaks due to impurities are observed in the calcined product, thus confirming the complete conversion to ZnO phase.

In terms of morphology, the ZnO precursor particles exhibit 3D wool-ball-like structures, which are assembled of two-dimensional (2D) plate-like structures with relatively smooth surfaces. The average diameter of the ZnO precursor is around 7-8 μm and the thickness of the composing plates varies from 200-300 nm. Following calcination, the wool-ball-like structure is well-retained; however the average diameter is slightly decreased to around 6 μm (Fig. 2b). Moreover, the TEM images depicted in Fig. 2d and e clearly reveal the porous nature of the synthesized wool-ball-like ZnO particles, which can be attributed to the decomposition of the organic constituents in the ZnO precursor particles during calcination. From Fig. 2c, it can be observed that the 2D plates (thicknesses ~200-300 nm) assembling the wool-ball-like structures are composed of many small hexagonal-shaped nanoparticles with sizes in the range of 50-60 nm (Fig. 2e). The HRTEM image of the hexagonal plate-like nanoparticles assembling the 3D wool-ball-like ZnO (Fig. 2f) shows clear lattice fringes with *d*-spacing of 0.28 nm, which correspond to the *d*-spacing of (100) plane of ZnO.

In order to gain insight into the formation mechanism of the 3D wool-ball-like ZnO precursor particles, the effects of important parameters, such as reaction time and amount of glycerol were investigated. As depicted in Fig. S4a (Supporting Information), the product obtained at a short reaction time of 2 h consists of incompletely formed wool-ball-like particles. Furthermore, some nanoparticles can be observed on the surface of these particles, suggesting that they are still in the midst of self-organizing into 2D plate-like sub-units which assemble the 3D wool-ball-like structures. As the reaction time is prolonged to 4-8 h, these small nanoparticles fused together to form plate-like sub-units, however, a few of them has not yet perfectly assembled to form the wool-ball-like structures (Fig. S4b and S4c, Supporting Information).

ACCEPTED MANUSCRIPT

When the reaction time is further increased to 16 h, uniform and well-defined 3D wool-ball-like particles assembled by 2D plate-like particles are obtained (Fig. S4d, Supporting Information). At this particular reaction time, the plates assembling the wool-ball-like structures are sufficiently separated from each other and more spaces are observed between them. As such, a reaction time of 16 h is identified as the optimum reaction time for obtaining well-defined 3D wool-ball-like ZnO precursor particles.

The role of glycerol in the formation of the 3D wool-ball-like ZnO precursor particles was also investigated as shown in Fig. S5 (Supporting Information). From Fig. S5a, it can be seen that in the absence of glycerol, cauliflower-like particles composed of connecting hemispheres are obtained. This phenomenon suggests that the solvent 2-propanol may play an important role in the formation of spherical particles which form the foundation of the 3D wool-ball-like structures. In the proposed reaction system, glycerol is important for promoting the self-assembly or organization of the 2D plate-like sub-units into 3D wool-ball-like structures. This is particularly evident from the SEM images shown in Fig. S5b-d (Supporting Information), in which the increased addition of glycerol causes a gradual increase in the density of the plate-like sub-units to form more well-defined 3D wool-ball-like structures. Based on these results, a formation mechanism is proposed, as schematically illustrated in Fig. 2g. In the synthesis process, the mixing of glycerol with 2-propanol results in the formation of a quasi-microemulsion.[44] As glycerol tends to self-aggregate in polar solvents such as 2-propanol, micro-heterogeneities are generated in the reaction system.[45, 46] Furthermore, glycerol might also be partly polymerized under solvothermal conditions, thus giving rise to emulsified spheres. The ZnO precursor (identified by XRD to $Zn(OH)_2$ and $Zn_5(CO_3)_2(OH)_6$) nanoparticles, formed via the hydrolysis of zinc nitrate would crystallize and self-assemble to form 2D plate-like particles and with extended solvothermal treatment time, these plate-like sub-units would self-organize to form 3D wool-ball-like particles.

The XRD patterns of the wool-ball-like ZnO following modifications with MWCNTs are given in Fig. 1a (ii-iv). It can be observed that the wool-ball-like ZnO/MWCNTs composites with different ratios (10:1. 5:1, and 3:1) exhibit similar XRD patterns as the pure wool-ball-like ZnO. As seen in Fig. 1a (v), the pure MWCNTs sample shows a major peak at 26°, which corresponds to the (002) plane of graphite.[47] The absence of the peak of MWCNTs in the XRD patterns of the wool-ball-like ZnO/MWCNTs composites is likely due to its small concentration (<5 wt%), and hence, was not detected by XRD. In this work, we used atomic percent for each composition and the conversion to the weight percent

ACCEPTED MANUSCRIPT

of MWCNTs are 0.014%, 0.03%, and 0.04% for wool-ball-like ZnO/MWCNTs (10:1), (5:1), and (3:1) composites, respectively.

The SEM images of the wool-ball-like ZnO precursor/MWCNTs (10:1) composite (Fig. 3a and 3b) shows some MWCNTs with diameters of ~40-50 nm which are attached on the surface of the wool-ball-like particles. Following calcination at 350 °C for 2 h, the MWCNTs become slightly diffused onto the surface of wool-ball-like ZnO, and few ZnO nanoparticles are attached on the walls of the MWCNTs (Fig. 3c). This is likely due to the functionalization process of MWCNTs, which generated carboxyl and hydroxyl groups on the surface of the MWCNTs, which may have attracted the MWCNTs to attach on the surface of the wool-ball-like ZnO particles. When the ZnO:MWCNTs ratio is increased to 5:1 (Fig. 3d) or 3:1 (Fig. 3g), more MWCNTs can obviously be observed on the surface of the wool-ball-like particles and after the heat treatment, many ZnO nanoparticles become attached on the walls of the MWCNTs (Fig. 3e and 3f).

The most interesting phenomenon, however is observed for the ZnO/MWCNTs (3:1) composite following calcination, in which many tiny nanorods with lengths and widths of 50-60 nm and 18-22 nm, respectively, can be seen protruding from the surface of the 2D plate-like sub-units which assemble the 3D wool-ball-like structures (Fig. 3h and 3i and Fig. 4a-e). Such a unique observation may be attributed to the catalytic effect of MWCNTs, which could accelerate the growth or promote the fusing of the small ZnO nanoparticles into many tiny nanorods during calcination.[48] The HRTEM image of a typical wool-ball-like ZnO/MWCNTs composite (Fig. 4f) indicates the presence of lattice fringes in the hexagonal-shaped ZnO nanoparticles with *d*-spacing of 0.28 nm, corresponding to the (001) plane of ZnO as well as the (002) plane of graphitic carbon in the MWCNT (*d*-spacing = 0.334 nm). To further confirm the composition of the wool-ball-like ZnO/MWCNTs composites, TEM-EDS analysis was carried out. The presence of Zn, O, and C elements can be clearly observed in all the composites, as depicted in Fig. S6a-l (Supporting Information).

Surface area and porosity are key parameters which may affect the sensing performance of nanomaterials as they govern the availability of active sites for the adsorption of gas molecules and the rate of diffusion of gas molecules. Fig. 5 presents the N_2 adsorption-desorption isotherms of the 3D wool-ball-like ZnO and wool-ball-like ZnO/MWCNTs composites with different ratios of ZnO:MWCNTs. Evidently, all the samples exhibit type IV isotherms, which are characteristic of mesoporous materials. Based on our previous report, the MWCNTs has a high specific surface area of 153.06 $m^2 g^{-1}$.[47] In comparison, the specific surface area of the wool-ball-like ZnO (30.5 $m^2 g^{-1}$) is considerably lower than the MWCNTs. The presence of MWCNTs can increase the adsorption of the wool-ball-like ZnO, leading to an

ACCEPTED MANUSCRIPT

increase in surface area. Specifically, the BET specific surface area values of the ZnO/MWCNTs (10:1), (5:1), and (3:1) composites are 42.1, 53.0, and 58.3 $m^2 g^{-1}$, respectively.

3.2 Gas-sensing performance

Inspired by the unique wool-ball-like morphology of the ZnO/MWCNTs composites, we have tested them as sensing materials for the detection of toxic SO_2 gas, which is one of the most common air pollutants. The operating temperature is one of the most significant factors affecting the gas-sensing performance as it determines the mobility of electrons and hence, the conductivity of the material.[49] Fig. 6a shows the variations in responses of the wool-ball-like ZnO and wool-ball-like ZnO/MWCNTs sensors to 70 ppm of SO_2 with increasing operating temperatures from 150° to 400 °C. It can be observed that the pure wool-ball-like ZnO sensor does not show any response to SO_2 gas up until the temperature reaches 250 °C, where it shows a high sensing response of 74.08. The response of the pure wool-ball-like ZnO sensor continues to increase with the increase in temperature before it reaches a maximum value of 150.6 at 350 °C. However, with a further increase in temperature to 400 °C, the response decreases to 102.6, suggesting that the surface desorption process of SO_2 gas becomes the more dominant reaction at such temperatures.

In comparison to the pure ZnO sensor, the wool-ball-like ZnO/MWCNTs (10:1) sensor exhibits an already high response of 56.4 to 70 ppm of SO_2 at a low temperature of 200 °C, and the response gradually increases until it reaches a maximum value of 220.8 at an optimum operating temperature of 300 °C. This response value is approximately three times higher than that of the pure wool-ball-like ZnO sensor at 300 °C. When the operating temperatures were raised to 350 °C and 400 °C, the responses sharply decrease to 99.7 and 28.7, respectively. Interestingly, the addition of more MWCNTs does not necessarily improve the sensing response but rather decreases the response, although both wool-ball-like ZnO/MWCNTs (5:1) and (3:1) sensors display some response to 70 ppm of SO_2 at 150 °C, while the pure wool-ball-like ZnO sensor does not show any response. The wool-ball-like ZnO/MWCNT (5:1) composite shows a moderate sensing response of 31.2 to 70 ppm of SO_2 at an optimum operating temperature of 300 °C, while the ZnO/MWCNT (3:1) composite displays a relatively low response of 6.75 at an optimum operating temperature of 350 °C.

Fig. 6b displays the responses of the wool-ball-like ZnO and wool-ball-like ZnO/MWCNTs sensors to different concentrations of SO_2 at 300 °C. Evidently, the pure wool-ball-like ZnO sensor shows only slightly different responses with different SO_2 concentrations, which suggests the occurrence of surface saturation. In comparison, regardless of the

ACCEPTED MANUSCRIPT

ratios of ZnO:MWCNTs, all the ZnO/MWCNTs sensors exhibit similar sensing behaviors, in which the response increases with the increase in SO_2 concentration. At a low SO_2 concentration, the response is lower because only a small amount of SO_2 interacts with the active sites on the surface of the wool-ball-like ZnO/MWCNTs particles. However, as the SO_2 concentration is increased, more SO_2 gas molecules are adsorbed on the surface, leading to a higher sensing response. Among the composite sensors, the wool-ball-like ZnO/MWCNTs (10:1) sensor shows the best sensing performance, with the response values being 73.4, 123.8, 144.7, 203.7, 220.8, and 270.5 to 2, 10, 30, 50, 70, and 100 ppm of SO_2, respectively. The fact that the sensing response of this composite sensor is still very high at 2 ppm of SO_2 suggests that this sensor is likely to have detection limit in the tens or hundreds of ppb level. In contrast, both ZnO/MWNCTs (5:1) and (3:1) sensors show worse performance than the pure ZnO sensor. This is because in the fabricated ZnO/MWCNTs composites, ZnO is the main sensing material and the increased amount of MWCNTs may cover or reduce the active sites available for the adsorption of gas molecules on the surface of the wool-ball-like ZnO particles, leading to a poorer sensing performance. The effect of relative humidity on the SO_2 sensing performance of the ZnO/MWCNT (3:1) sensor is presented in Fig. S7 (Supporting Information). Evidently, the sensing response gradually decreases with increasing humidity. This may be attributed to the increased presence of moisture adsorbed on the ZnO surface at higher humidity level which can inhibit the adsorption of oxygen and SO_2 molecules, thereby lowering the overall sensing response.[10, 33]

The response time is defined as the time required by the sensor to reach 90% of its maximum response following an exposure to a particular gas, whereas the recovery time is defined as the time required for the sensor to reach 90% of its original conductance following removal of the gas. The dynamic response-recovery curves of the pure wool-ball-like ZnO and wool-ball-like ZnO/MWCNTs sensors to various concentrations of SO_2 (from 2-100 ppm) at 300 °C are given in Fig. S8 (Supporting Information). Evidently, all the sensors exhibit the typical *n*-type sensing behaviors, whereby the resistance decreases as SO_2 gas is introduced and subsequently decreases as the gas is removed. The response time values of the pure wool-ball-like ZnO sensor to 2, 10, 20, 30, 50, 70, and 100 ppm of SO_2 are 255, 250, 195, 190, 175, and 180 s, respectively (Fig. 6c). In comparison, the response time values for the wool-ball-like ZnO/MWCNTs (3:1) composite are 330, 250, 210, 255, 205, and 235 s, respectively, while the response time values for the ZnO/MWCNTs (5:1) composite are 70, 95, 90, 50, 60, and 100 s, respectively. Among these sensors, the ZnO/MWCNTs (10:1) composite exhibits the fastest response speed with the values being 65, 60, 50 40, 60, and 45 s to 10, 20, 30, 50, 70, and 100 ppm of SO_2,

ACCEPTED MANUSCRIPT

respectively. On the other hand, the trend in recovery time is in the order of: pure ZnO < ZnO/MWCNTs (10:1) < ZnO/MWCNTs (5:1) < ZnO/MWCNTs (3:1), as shown in Fig. 6d. In previous reports, pristine MWCNTs sensors have been reported to suffer from sluggish response and/or recovery time(s).[38, 50] However, in this study, the wool-ball-like ZnO/MWCNTs (10:1) sensor shows fast response speed with acceptable recovery time. The improved response/recovery speed of this composite sensor may be attributed to the synergistic effect between the ZnO and MWCNTs which could accelerate the kinetics of surface adsorption of O_2 and SO_2 molecules during the sensing process.[51]

Stability is another crucial parameter in gas-sensing as it determines the long-term operation potential of the sensor. As such, we investigated the sensing performance of the wool-ball-like ZnO/MWCNTs (10:1) sensor once a day for 7 consecutive days. As evident in Fig. 7a**,** the fabricated ZnO/MWCNTs (10:1) sensor shows a high stability for SO_2 gas detection as the change in its resistance follows a relatively similar pattern each day and no significant drop in the sensing performance is observed. Apart from exhibiting high stability, an ideal sensing material has the capability to selectively detect a particular gas when it is exposed to an environment containing several gases with nearly identical physicochemical properties. Fig. 7b displays the selectivity test results of the pure wool-ball-like ZnO and wool-ball-like ZnO/MWCNTs sensors to 50 ppm of different gases, including CO, CO_2, SO_2, methanol, hexane, xylene, and toluene, at 300 °C. Evidently, the pure wool-ball-like ZnO sensor still exhibits some cross sensitivity to CO and CO_2 gases, and therefore, its selectivity is not as satisfactory. Similarly, the wool-ball-like ZnO/MWCNTs (5:1) and (3:1) sensors also do not show satisfactory selectivity to SO_2 as the response is roughly only double of those of other gases. However, unlike these sensors, the wool-ball-like ZnO/MWCNTs (10:1) sensor displays excellent selectivity to SO_2 gas as the response to SO_2 (50 ppm) is approximately 7-14 times higher than the responses to other gases at a similar concentration level. The improved selectivity of the ZnO/MWCNTs composite may be attributed to the presence of functional groups (carboxyl and hydroxyl) on the surface of the MWCNTs following the functionalization process, which assisted in the screening of multiple analytes.[51] Table 1 compares the SO_2 sensing performance of the fabricated wool-ball-like ZnO/MWCNT (10:1) composite against previously reported semiconducting metal oxide nanostructures. It is evident from this table that the wool-ball-like ZnO/MWCNTs (10:1) composite shows significantly better SO_2 sensing performance than previous sensors made of pure and Ag-loaded WO_3,[52, 53] pure and V_2O_5-loaded SnO_2,[54, 55] as well as 1D MCo_2O_4 (M = Ni, Cu, Zn) nanostructures.[56]

3.3 Gas-sensing mechanism

ACCEPTED MANUSCRIPT

In this study, all the sensors including the wool-ball-like ZnO/MWCNT sensors exhibit *n*-type sensing behavior, where the resistance decreases following exposure to a reducing gas such as SO_2. As discussed earlier, ZnO is the main sensing material in the wool-ball-like ZnO/MWCNTs sensors and as such, the composite sensors follow the behavior of ZnO, which is an *n*-type sensing material. A schematic illustration of the gas-sensing mechanism of the wool-ball-like ZnO sensor is given in Fig. 8a. In the case of pure ZnO sensor, the interaction between the ZnO surface and SO_2 gas mainly occurs through chemisorption, which involves the oxygen ionosorption process. The chemisorption of oxygen (O_2) typically starts at 75 °C, because at such temperature, oxygen has sufficient energy to overcome the activation energy. Below 150°C, O_2 will adsorb on the surface, dissociate, and ionized by taking electron(s) from the conduction band of ZnO to form O_2^-. In the temperature range of 150-200 °C, O_2^- starts to disappear and O^- becomes the predominant oxygen species. When temperature is raised above 200 °C, O^- gradually disappears and O^{2-} becomes more pronounced on the surface of ZnO.[10, 57-59] The overall process can be represented by the following equations:

$$O_2\,(gas) \Leftrightarrow O_2\,(ads) \quad (1)$$

$$O_2\,(ads) + e^- \Leftrightarrow O_2^-\,(ads) \quad (2)$$

$$O_2^-\,(ads) + e^- \Leftrightarrow 2O^-\,(ads) \quad (3)$$

$$O^- + e^- \Leftrightarrow O^{2-}\,(ads) \quad (4)$$

As electrons are taken from ZnO during the chemisorption of oxygen, an electron depletion layer is created which increases the resistance of ZnO. Next, when SO_2 is introduced into the chamber, it adsorbs on the surface of ZnO and mostly interacts with O^{2-} (the predominant oxygen species at 300 °C, which is our optimum operating temperature) to form SO_3, according to Eq. 5[1, 57]:

$$SO_2 + O^{2-}\,(ads) \rightarrow SO_3 + 2e^- \quad (5)$$

This reaction releases electrons back to the conduction band of ZnO, thus narrowing the depletion layer, which in turn decreases the overall resistance of the sensor. Following exposure to air, oxygen chemisorption occurs and the resistance of the ZnO sensor returns to the original baseline value. Our previous density functional theory (DFT) study has demonstrated the strong adsorption of SO_2 on ZnO(0002) surface by forming chemical bonding with O atom on the surface of ZnO to form SO_3, whereas gases such as CO_2 and NO only physically adsorbed or bound to the surface of ZnO.[60] The formation of SO_3 has also been observed experimentally in our previous work, in which sulfuric acid

ACCEPTED MANUSCRIPT

originating from the reaction between SO_3 and water vapour was detected in the exhaust of the gas sensor instrument during the sensing test.[61]

The enhanced sensing performance of the wool-ball-like ZnO/MWCNTs (10:1) composite compared to the pure wool-ball-like ZnO sensor may be attributed to several factors. First, the combination of MWCNTs with ZnO leads to a larger surface area as seen in Fig. 5 and this facilitates the creation of more active sites for the adsorption of gas molecules. Second, the small ZnO NPs assembling the wool-ball-like structures may provide a spillover effect (similar to metal nanoparticles) which can enhance the adsorption, dissociation, and migration of gas molecules. Third, the presence of functional groups on the surface of MWCNTs introduced *via* covalent functionalization during the synthesis process may help to create defect sites, which in turn, provide additional sites for the adsorption of O_2 and SO_2 molecules. This explanation is supported by a previous report which demonstrated the superior sensitivity of carboxyl and hydroxyl-modified CNTs to SO_2 when compared with pristine CNTs, as a result of the increased number of defect sites.[51]

Furthermore, MWCNTs have been reported to behave like a *p*-type semiconductor with holes as the major charge carriers, whereas ZnO acts as an *n*-type semiconductor with electrons as the major charge carriers. Therefore, many *p*-*n* heterojunctions are formed at the ZnO/MWCNTs interfaces (Fig. 8b).[38, 62] In addition, the lower work function (φ) of MWCNTs (φCNT = 4.7– 4.9 eV) compared to ZnO (φZnO = 5.1–5.4 eV) leads to the formation of Ohmic contacts between ZnO and MWCNTs.[38, 40, 63] However, as the difference in their work functions is relatively small, the interfacial barrier between these two materials is rather low. Due to the creation of a *p*-*n* heterojunction, as well as the lower work function of MWCNTs relative to ZnO, electrons will energetically transfer from the conduction band of ZnO to MWCNTs and holes will flow from MWCNTs to ZnO, until the formed built-in potential prevents further flow of electrons and holes.[38, 62] Hence, the hole concentration in the MWCNTs and electron concentration in ZnO will be reduced. Accordingly, the width of the hole accumulation layer in the MWCNT will be decreased underneath the ZnO, and the hole conduction channel is greatly decreased.[38] Consequently, this results in a major increase in the resistance of the MWCNTs. In the presence of air, the hole accumulation layer is heavily suppressed by the ZnO. However, when SO_2 gas is introduced, it will be enlarged, and the electrical resistance decreases owing to the easy flow of the hole carriers. However, the ratio of resistance changes is far greater for the ZnO/MWCNTs (10:1) sensor compared to the pristine ZnO sensor, which therefore, leads to a much higher sensing response.

ACCEPTED MANUSCRIPT

4. Conclusions

In summary, this study reports the facile synthesis of hierarchical 3D wool-ball-like ZnO nanostructures using a glycerol-assisted solvothermal method for followed by a subsequent calcination in air at 350 °C. Glycerol is found to play an important role in promoting the self-assembly of the 2D plate-like sub-units into 3D wool-ball-like particles as the increase in the amount of glycerol leads to a gradual increase in the density of the plate-like sub-units to form more well-defined 3D wool-ball-like structures. Following modifications with MWCNTs, MWCNTs with an average diameter of around 80 nm are attached on the surface of the wool-ball-like ZnO particles. However, a very interesting phenomenon is observed with the wool-ball-like ZnO/MWCNTs (3:1) composite, in which numerous small nanorods grew on the surface of the 2D plate-like sub-units which assemble the 3D wool-ball-like particles. The formation of these small nanorods may be contributed by the catalytic effect of MWCNTs, which could accelerate the growth or promote the fusing of the small ZnO nanoparticles into nanorods during heat treatment. When evaluated for SO_2 sensing, the wool-ball-like ZnO/MWCNTs (10:1) composite shows the highest sensing performance among all the tested sensors, with the response being as high as 221 when exposed to 70 ppm of SO_2 at an optimum temperature of 300 °C. This response value is roughly three times higher than that of the pure wool-ball-like ZnO sensor. In addition, the wool-ball-like ZnO/MWCNTs (10:1) composite also displays high stability and good selectivity to SO_2 with the response to SO_2 being 7-14 times higher than the responses to other tested gases at a similar concentration of 50 ppm. The significant improvement in the sensing performance of the wool-ball-like ZnO/MWCNTs (10:1) composite compared to the pure wool-ball-like ZnO is largely due to two main factors: (i) the formation of *p-n* heterojunctions at the ZnO/MWCNTs interfaces, which greatly enhance the ratio of resistance changes of the composite sensor upon exposure to SO_2 gas and (ii) the increased amount of active sites available for the adsorption of gases owing to the larger surface area of the composite and the presence of defect sites on the surface of the MWCNTs introduced through the functionalization process.

Acknowledgments

This work was partially supported by The Financial Ministry of Indonesia (LPDP). Y. V. Kaneti thanks the Japan Society for Promotion of Science (JSPS) for providing the standard postdoctoral fellowship. The authors also acknowledged the financial assistance from World Class University (WCU) and World Class Professor (WCP) program.

ACCEPTED MANUSCRIPT

References

[1] K. Wetchakun, T. Samerjai, N. Tamaekong, C. Liewhiran, C. Siriwong, V. Kruefu, A. Wisitsoraat, A. Tuantranont, S. Phanichphant, Semiconducting metal oxides as sensors for environmentally hazardous gases, Sens. Actuator B, 160(2011) 580-591.
[2] P. Tyagi, A. Sharma, M. Tomar, V. Gupta, Efficient detection of SO_2 gas using SnO_2 based sensor loaded with metal oxide catalysts, Procedia Eng., 87(2014) 1075-1078.
[3] P. Tyagi, A. Sharma, M. Tomar, V. Gupta, A comparative study of RGO-SnO_2 and MWCNT-SnO_2 nanocomposites based SO_2 gas sensors, Sens. Actuator B, 248(2017) 980-986.
[4] J.F.d.S. Petruci, A. Wilk, A.A. Cardoso, B. Mizaikoff, Online analysis of H_2S and SO_2 via advanced mid-infrared gas sensors, Anal. Chem., 87(2015) 9605-9611.
[5] M. Nonomura, T. Hobo, Simultaneous determination of sulphur oxides, nitrogen oxides and hydrogen chloride in flue gas by means of an automated ion chromatographic system, J. Chrom. A, 804(1998) 151-155.
[6] V.B. Raj, A.T. Nimal, Y. Parmar, M.U. Sharma, K. Sreenivas, V. Gupta, Cross-sensitivity and selectivity studies on ZnO surface acoustic wave ammonia sensor, Sens. Actuator B, 147(2010) 517-524.
[7] F.W. Koehler, G.W. Small, R.J. Combs, R.B. Knapp, R.T. Kroutil, Automated detection of sulfur dioxide in stack emissions by passive Fourier transform infrared spectrometry, Vibrat. Spectrosc., 27(2001) 97-107.
[8] C.J. Martinez, B. Hockey, C.B. Montgomery, S. Semancik, Porous tin oxide nanostructured microspheres for sensor applications, Langmuir, 21(2005) 7937-7944.
[9] E.R. Leite, I.T. Weber, E. Longo, J.A. Varela, A new method to control particle size and particle size distribution of SnO_2 nanoparticles for gas sensor applications, Adv. Mater., 12(2000) 965-968.
[10] Y.V. Kaneti, J. Yue, X. Jiang, A. Yu, Controllable synthesis of ZnO nanoflakes with exposed $(10\bar{1}0)$ for enhanced gas sensing performance, J. Phys. Chem. C, 117(2013) 13153-13162.
[11] C. Shoou-Jinn, H. Ting-Jen, I.C. Chen, H. Bohr-Ran, Highly sensitive ZnO nanowire CO sensors with the adsorption of Au nanoparticles, Nanotechnology, 19(2008) 175502.
[12] X. Yang, V. Salles, Y.V. Kaneti, M. Liu, M. Maillard, C. Journet, X. Jiang, A. Brioude, Fabrication of highly sensitive gas sensor based on Au functionalized WO_3 composite nanofibers by electrospinning, Sens. Actuator B, 220(2015) 1112-1119.
[13] Y.S. Kim, S.-C. Ha, K. Kim, H. Yang, S.-Y. Choi, Y.T. Kim, J.T. Park, C.H. Lee, J. Choi, J. Paek, K. Lee, Room-temperature semiconductor gas sensor based on nonstoichiometric tungsten oxide nanorod film, Appl. Phys. Lett., 86(2005) 213105.
[14] J. Bai, B. Zhou, Titanium dioxide nanomaterials for sensor applications, Chem. Rev., 114(2014) 10131-10176.
[15] P. Maggie, K.V. Oomman, K.M. Gopal, A.G. Craig, G.O. Keat, Unprecedented ultra-high hydrogen gas sensitivity in undoped titania nanotubes, Nanotechnology, 17(2006) 398.
[16] Y.V. Kaneti, Z. Zhang, J. Yue, Q.M.D. Zakaria, C. Chen, X. Jiang, A. Yu, Crystal plane-dependent gas-sensing properties of zinc oxide nanostructures: experimental and theoretical studies, Phys. Chem. Chem. Phys., 16(2014) 11471-11480.
[17] J. Kim, K. Yong, Mechanism study of ZnO nanorod-bundle sensors for H_2S gas sensing, J. Phys. Chem. C, 115(2011) 7218-7224.
[18] L. Chow, O. Lupan, H. Heinrich, G. Chai, Self-assembly of densely packed and aligned bilayer ZnO nanorod arrays, Appl. Phys. Lett., 94(2009) 163105.
[19] L. Vayssieres, Growth of arrayed nanorods and nanowires of ZnO from aqueous solutions, Adv. Mater., 15(2003) 464-466.
[20] Y. Sun, D.J. Riley, M.N.R. Ashfold, Mechanism of ZnO nanotube growth by hydrothermal methods on ZnO film-coated Si substrates, J. Phys. Chem. B, 110(2006) 15186-15192.
[21] Z. Jing, J. Zhan, Fabrication and gas-sensing properties of porous ZnO nanoplates, Adv. Mater., 20(2008) 4547-4551.
[22] M. Chen, Z. Wang, D. Han, F. Gu, G. Guo, Multiwalled carbon nanotubes – zinc oxide nanocomposites as low temperature toluene gas sensor, J. Phys. Chem. C, 115(2011) 12763-12773.
[23] S.J. Chen, Y.C. Liu, C.L. Shao, R. Mu, Y.M. Lu, J.Y. Zhang, D.Z. Shen, X.W. Fan, Structural and optical properties of uniform ZnO nanosheets, Adv. Mater., 17(2005) 586-590.
[24] J.-H. Park, H.-J. Choi, Y.-J. Choi, S.-H. Sohn, J.-G. Park, Ultrawide ZnO nanosheets, J. Mater. Chem., 14(2004) 35-36.
[25] Y. Sun, L. Wang, X. Yu, K. Chen, Facile synthesis of flower-like 3D ZnO superstructures via solution route, CrystEngComm, 14(2012) 3199-3204.

ACCEPTED MANUSCRIPT

[26] H. Zhang, R. Wu, Z. Chen, G. Liu, Z. Zhang, Z. Jiao, Self-assembly fabrication of 3D flower-like ZnO hierarchical nanostructures and their gas sensing properties, CrystEngComm, 14(2012) 1775-1782.
[27] J. Elias, C. Lévy-Clément, M. Bechelany, J. Michler, G.-Y. Wang, Z. Wang, L. Philippe, Hollow urchin-like ZnO thin films by electrochemical deposition, Adv. Mater., 22(2010) 1607-1612.
[28] F. Meng, J. Yin, Y.-Q. Duan, Z.-H. Yuan, L.-J. Bie, Co-precipitation synthesis and gas-sensing properties of ZnO hollow sphere with porous shell, Sens. Actuator B, 156(2011) 703-708.
[29] J. Zhao, X. Zou, L.-J. Zhou, L.-L. Feng, P.-P. Jin, Y.-P. Liu, G.-D. Li, Precursor-mediated synthesis and sensing properties of wurtzite ZnO microspheres composed of radially aligned porous nanorods, Dalton Trans., 42(2013) 14357-14360.
[30] W. Li, X. Wu, N. Han, J. Chen, X. Qian, Y. Deng, W. Tang, Y. Chen, MOF-derived hierarchical hollow ZnO nanocages with enhanced low-concentration VOCs gas-sensing performance, Sens. Actuator B, 225(2016) 158-166.
[31] D.R. Miller, S.A. Akbar, P.A. Morris, Nanoscale metal oxide-based heterojunctions for gas sensing: a review, Sens. Actuator B, 204(2014) 250-272.
[32] C. Liu, Q. Kuang, Z. Xie, L. Zheng, The effect of noble metal (Au, Pd and Pt) nanoparticles on the gas sensing performance of SnO_2-based sensors: a case study on the {221} high-index faceted SnO_2 octahedra, CrystEngComm, 17(2015) 6308-6313.
[33] Y.V. Kaneti, J. Yue, J. Moriceau, C. Chen, M. Liu, Y. Yuan, X. Jiang, A. Yu, Experimental and theoretical studies on noble metal decorated tin oxide flower-like nanorods with high ethanol sensing performance, Sens. Actuator B, 219(2015) 83-93.
[34] J. Ding, J. Zhu, P. Yao, J. Li, H. Bi, X. Wang, Synthesis of ZnO–Ag hybrids and their gas-sensing performance toward ethanol, Ind. Eng. Chem. Res., 54(2015) 8947-8953.
[35] O. Lupan, V. Cretu, V. Postica, M. Ahmadi, B.R. Cuenya, L. Chow, I. Tiginyanu, B. Viana, T. Pauporté, R. Adelung, Silver-doped zinc oxide single nanowire multifunctional nanosensor with a significant enhancement in response, Sens. Actuator B, 223(2016) 893-903.
[36] N. Tamaekong, C. Liewhiran, A. Wisitsoraat, S. Phanichphant, Acetylene sensor based on Pt/ZnO thick films as prepared by flame spray pyrolysis, Sens. Actuator B, 152(2011) 155-161.
[37] Y. Zhang, Q. Xiang, J. Xu, P. Xu, Q. Pan, F. Li, Self-assemblies of Pd nanoparticles on the surfaces of single crystal ZnO nanowires for chemical sensors with enhanced performances, J. Mater. Chem., 19(2009) 4701-4706.
[38] Y.J. Kwon, A. Mirzaei, S.Y. Kang, M.S. Choi, J.H. Bang, S.S. Kim, H.W. Kim, Synthesis, characterization and gas sensing properties of ZnO-decorated MWCNTs, Appl. Surf. Sci., 413(2017) 242-252.
[39] F. Schütt, V. Postica, R. Adelung, O. Lupan, Single and networked ZnO–CNT hybrid tetrapods for selective room-temperature high-performance ammonia sensors, ACS Appl. Mater. Interfaces, 9(2017) 23107-23118.
[40] A. Ahmed, A. Alaa, S. Giuseppe, L. Paolo, Metallic nanoparticles functionalizing carbon nanotube networks for gas sensing applications, Nanotechnology, 25(2014) 055208.
[41] G. Huang, F. Zhang, X. Du, Y. Qin, D. Yin, L. Wang, Metal organic frameworks route to in situ insertion of multiwalled carbon nanotubes in Co_3O_4 polyhedra as anode materials for lithium-ion batteries, ACS Nano, 9(2015) 1592-1599.
[42] M. Najafi, H. Haratizadeh, Investigation of intrinsic and extrinsic defects effective role on producing intense red emission in ZnO:Eu nanostructures, Mater. Res. Bull., 65(2015) 103-109.
[43] H. Jaeeun, P. Jaehoon, K. Hongdoo, UV-assisted rapid thermal annealing for solution-processed zinc oxide thin-film transistors, Semicond. Sci. Technol., 29(2014) 095019.
[44] B. Wang, J.S. Chen, H.B. Wu, Z. Wang, X.W. Lou, Quasiemulsion-templated formation of α-Fe_2O_3 hollow spheres with enhanced lithium storage properties, J. Am. Chem. Soc., 133(2011) 17146-17148.
[45] A.B. Roney, B. Space, E.W. Castner, R.L. Napoleon, P.B. Moore, A molecular dynamics study of aggregation phenomena in aqueous n-propanol, J. Phys. Chem. B, 108(2004) 7389-7401.
[46] A. Idrissi, S. Longelin, The study of aqueous isopropanol solutions at various concentrations: low frequency raman spectroscopy and molecular dynamics simulations, J. Mol. Struc., 651(2003) 271-275.
[47] N.L.W. Septiani, B. Yuliarto, Nugraha, H.K. Dipojono, Multiwalled carbon nanotubes–zinc oxide nanocomposites as low temperature toluene gas sensor, Appl. Phys. A, 123(2017) 166.
[48] H. Dai, Carbon nanotubes: synthesis, integration, and properties, Acc. Chem. Res., 35(2002) 1035-1044.
[49] Y.V. Kaneti, Q.M.D. Zakaria, Z. Zhang, C. Chen, J. Yue, M. Liu, X. Jiang, A. Yu, Solvothermal synthesis of ZnO-decorated α-Fe_2O_3 nanorods with highly enhanced gas-sensing performance toward n-butanol, J. Mater. Chem. A, 2(2014) 13283-13292.

ACCEPTED MANUSCRIPT

[50] S.G. Wang, Q. Zhang, D.J. Yang, P.J. Sellin, G.F. Zhong, Multi-walled carbon nanotube-based gas sensors for NH_3 detection, Diamond Relat. Mater., 13(2004) 1327-1332.
[51] M. Mittal, A. Kumar, Carbon nanotube (CNT) gas sensors for emissions from fossil fuel burning, Sens. Actuator B, 203(2014) 349-362.
[52] C.M. Ghimbeu, M. Lumbreras, J. Schoonman, M. Siadat, Electrosprayed metal oxide semiconductor films for sensitive and selective detection of hydrogen sulfide, Sensors, 9(2009) 9122.
[53] Y. Shimizu, N. Matsunaga, T. Hyodo, M. Egashira, Improvement of SO_2 sensing properties of WO_3 by noble metal loading, Sens. Actuator B, 77(2001) 35-40.
[54] C. Liewhiran, N. Tamaekong, A. Wisitsoraat, S. Phanichphant, Highly selective environmental sensors based on flame-spray-made SnO_2 nanoparticles, Sens. Actuator B, 163(2012) 51-60.
[55] S. Das, S. Chakraborty, O. Parkash, D. Kumar, S. Bandyopadhyay, S.K. Samudrala, A. Sen, H.S. Maiti, Vanadium doped tin dioxide as a novel sulfur dioxide sensor, Talanta, 75(2008) 385-389.
[56] G.-Y. Zhang, B. Guo, J. Chen, MCo_2O_4 (M=Ni, Cu, Zn) nanotubes: template synthesis and application in gas sensors, Sens. Actuator B, 114(2006) 402-409.
[57] S.C. Chang, Oxygen chemisorption on tin oxide: Correlation between electrical conductivity and EPR measurements, J. Vac. Sci. Technol., 17(1980) 366-369.
[58] S. Lenaerts, J. Roggen, G. Maes, FT-IR characterization of tin dioxide gas sensor materials under working conditions, Spectrochim. Acta A, 51(1995) 883-894.
[59] Y.V. Kaneti, Z. Zhang, J. Yue, X. Jiang, A. Yu, Porous $FeVO_4$ nanorods: synthesis, characterization, and gas-sensing properties toward volatile organic compounds, J. Nanopart. Res., 15(2013) 1948.
[60] Nugraha, A.G. Saputro, M.K. Agusta, B. Yuliarto, H.K. Dipojono, R. Maezono, Density functional study of adsorptions of CO_2, NO_2 and SO_2 molecules on Zn(0002) surfaces, J. Phys. Conf. Ser., 739(2016) 012080.
[61] B. Yuliarto, M.F. Ramadhani, Nugraha, N.L.W. Septiani, K.A. Hamam, Enhancement of SO_2 gas sensing performance using ZnO nanorod thin films: the role of deposition time, J. Mater. Sci., 52(2017) 4543-4554.
[62] W. Lin, S. Huang, W. Chen, An MWCNT-doped SnO_2 thin film NO_2 gas sensor by RF reactive magnetron sputtering, J. Semicond., 31(2010) 024006.
[63] V. Postica, F. Schütt, R. Adelung, O. Lupan, Schottky diode based on a single carbon–nanotube–ZnO hybrid tetrapod for selective sensing applications, Adv. Mater. Interfaces, 4(2017) 1700507.
[64] H. Liu, Q. Zhou, Q. Zhang, C. Hong, L. Xu, L. Jin, W. Chen, Synthesis, characterization and enhanced sensing properties of a NiO/ZnO p–n junctions sensor for the SF_6 decomposition byproducts SO_2, SO_2F_2, and SOF_2, Sensors, 17(2017) 913.
[65] M. Stankova, X. Vilanova, J. Calderer, E. Llobet, P. Ivanov, I. Gràcia, C. Cané, X. Correig, Detection of SO_2 and H_2S in CO_2 stream by means of WO_3-based micro-hotplate sensors, Sens. Actuator B, 102(2004) 219-225.

ACCEPTED MANUSCRIPT

ACCEPTED MANUSCRIPT

AUTHOR BIOGRAPHIES

Dr. Yusuf Valentino Kaneti obtained his Ph.D. degree in 2014 from the University of New South Wales (UNSW), Australia. He is currently working as a JSPS postdoctoral fellow at the National Institute of Materials Science (NIMS), Japan. His research interest is on the fabrication of functional inorganic nanomaterials and nanocomposites for energy and environmental applications. He has published 37 journal articles and 1 book chapter, with citations of over 600, leading to a H-index of 14.

Ms. Ni Luh Wulan Septiani is a doctoral candidate studying at the Bandung Institute of Technology, Indonesia. Her doctoral project focuses on the synthesis, characterization and application of metal oxide nanostructures and nanocomposites for gas-sensing applications.

Dr. Nugraha received his Master and Ph.D. degrees from Tohoku University, Japan. He is now working as a lecturer at the Faculty of Industrial Technology, Bandung Institute of Technology, Indonesia. His research interest is on the experimental and theoretical studies of metal oxide nanostructures for gas-sensing applications.

Prof. Brian Yuliarto received his Master and Ph.D. degrees from the University of Tokyo, Japan. He is currently working as a full-time professor at the Faculty of Engineering Physics, Bandung Institute of Technology, Indonesia. His research focuses on the synthesis and application of metal oxide nanostructures and their composites for gas-sensing, energy and solar cell applications. He has published more than 60 papers during his research career.

Prof. Hermawan Kresno Dipojono obtained his Ph.D. degree in 1996 from the Ohio University, USA. He is currently working as a full-time professor at the Faculty of Industrial Technology, Bandung Institute of Technology, Indonesia. His research interest is on computational materials design and quantum engineering. He has published more than 80 research articles during his research career.

ACCEPTED MANUSCRIPT

Dr. Toshiaki Takei is a technical staff working for the Nanotechnology Innovation Station, Nanofabrication Group, and Research Network and Facility Services Division at the National institute of Materials Science (NIMS), Japan. He has extensive expertise on the use of electron microscopes for protein and nanomaterials analysis.

Dr. Jongmuk You received his Ph.D. degree in 2011 from Yonsei University, South Korea. He is now working as an Assistant Professor at the Kyung-Hee University, South Korea. His research interest is on the fabrication of functional polymers for fluorescence applications. He has published 50 journal articles with total citations of over 800 times, leading to a H-index of 16.

Prof. Yusuke Yamauchi received his Bachelor degree (2003), Master degree (2004), and Ph.D. (2007) from the Waseda University, Japan. After receiving his Ph.D., he joined the National Institute of Materials Science (NIMS), Japan to start his own research group. He led a big team of senior scientists, technical staffs, and more than 30 PhD students/Postdocs. In May 2017, he joined the University of Wollongong as a full professor. He concurrently serves as an honorary group leader of NIMS, a visiting/honorary professor at several universities. He has published more than 500 papers in international refereed journals with >20,000 citations (h-index > 70). He has been selected as one of the Highly-Cited Researchers in Chemistry in 2016 and 2017.

ACCEPTED MANUSCRIPT

ACCEPTED MANUSCRIPT

FIGURE CAPTIONS

Fig. 1. (a) Thermogravimetric analysis (TGA)-differential scanning calorimetric (DSC) curves of the ZnO precursor particles from room temperature to 800 °C under an air atmosphere. (b) XRD patterns of (i) standard JCPDS No. 36-1451 for wurtzite ZnO, (ii) pure wool ball-like ZnO and wool ball-like ZnO/MWCNTs composites with ZnO:MWCNTs ratios of (iii) 10:1, (iv), 5:1, and (v), 3:1, and (vi) 0:1 (pure MWCNTs).

Fig. 2. SEM images of (a) 3D wool-ball-like ZnO precursor obtained from the solvothermal reaction between zinc nitrate and glycerol in 2-propanol at 180 °C for 16 h. (b) Low and (c) high-magnification SEM images of the 3D wool ball-like ZnO particles achieved by the calcination of the wool-ball-like precursor particles at 350 °C for 2 h (inset showing the plate-like sub-unit which is assembled of many small nanoparticles). (d) Low and (e) high-magnification TEM, and (f) HRTEM images of the porous 3D wool-ball-like ZnO particles. (g) Schematic illustration showing the proposed formation mechanism of the wool-ball-like ZnO precursor particles.

Fig. 3. SEM images of the 3D wool-ball-like ZnO precursor/MWCNTs composites with ratios of (a) 10:1, (d) 5:1, and (g) 3:1, obtained using the proposed solvothermal approach at 180 °C for 16 h. The corresponding SEM images of the porous 3D wool-ball-like ZnO/MWCNTs composites with ratios of (b, c) 10:1, (e, f) 5:1, and (h, i) 3:1 achieved through the calcination of the wool-ball-like ZnO precursor/MWCNTs (10:1), (5:1), and (3:1) composites, respectively, in air at 350 °C for 2 h, under a slow heating rate of 1 °C min^{-1}.

Fig. 4. (a) Low and (b) high-magnification SEM images of the wool-ball-like ZnO/MWCNTs (3:1) particle. (c, d) High magnification SEM images showing the growth of many tiny nanorods on the 2D plate-like sub-units assembling the 3D wool-ball-like ZnO as well as the MWCNTs attached to the surface of the wool-ball-like ZnO. (e) TEM and (f) HRTEM images of the wool-ball-like ZnO/MWCNTs (3:1) composite particles.

Fig. 5. Nitrogen (N_2) adsorption-desorption isotherms of (a) wool-ball-like ZnO and wool-ball-like ZnO/MWCNTs composites with ZnO:MWCNTs ratios of (b) 10:1, (c) 5:1, and (d) 3:1.

Fig. 6. (a) Responses of the wool-ball-like ZnO and wool-ball-like ZnO/MWCNTs sensors to 70 ppm of SO_2 gas at different operating temperatures from 150-400 °C. (b) Responses of the wool-ball-like ZnO and wool-ball-like ZnO/MWCNTs sensors to different concentrations of SO_2 at 300 °C. (c) Response time different concentrations of SO_2.

Fig. 7. (a) Stability test results of the ZnO wool-ball-like/MWCNTs (10:1) sensor to 50 ppm of SO_2 for 7 consecutive days and (b) selectivity test results of the pure wool-ball-like ZnO and wool-ball-like ZnO/MWCNTs composites to 50 ppm of various gases at 300 °C.

ACCEPTED MANUSCRIPT

Fig. 8. Schematic ilustration showing the possible sensing mechanisms of (a) wool-ball-like ZnO and (b) wool-ball-like ZnO/MWCNTs composite.

ACCEPTED MANUSCRIPT

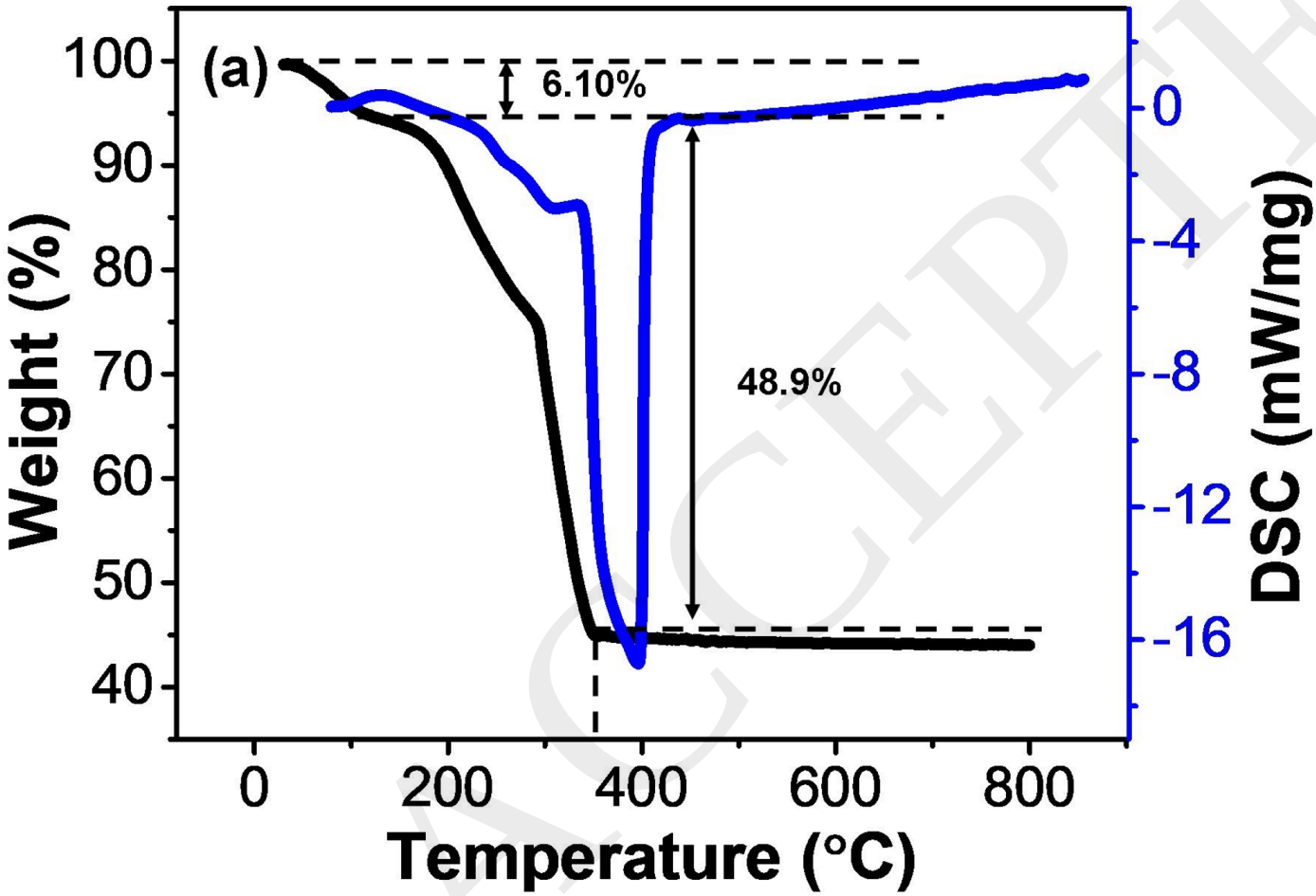
(a)
6.10%
48.9%
Weight (%)
DSC (mW/mg)
Temperature (°C)

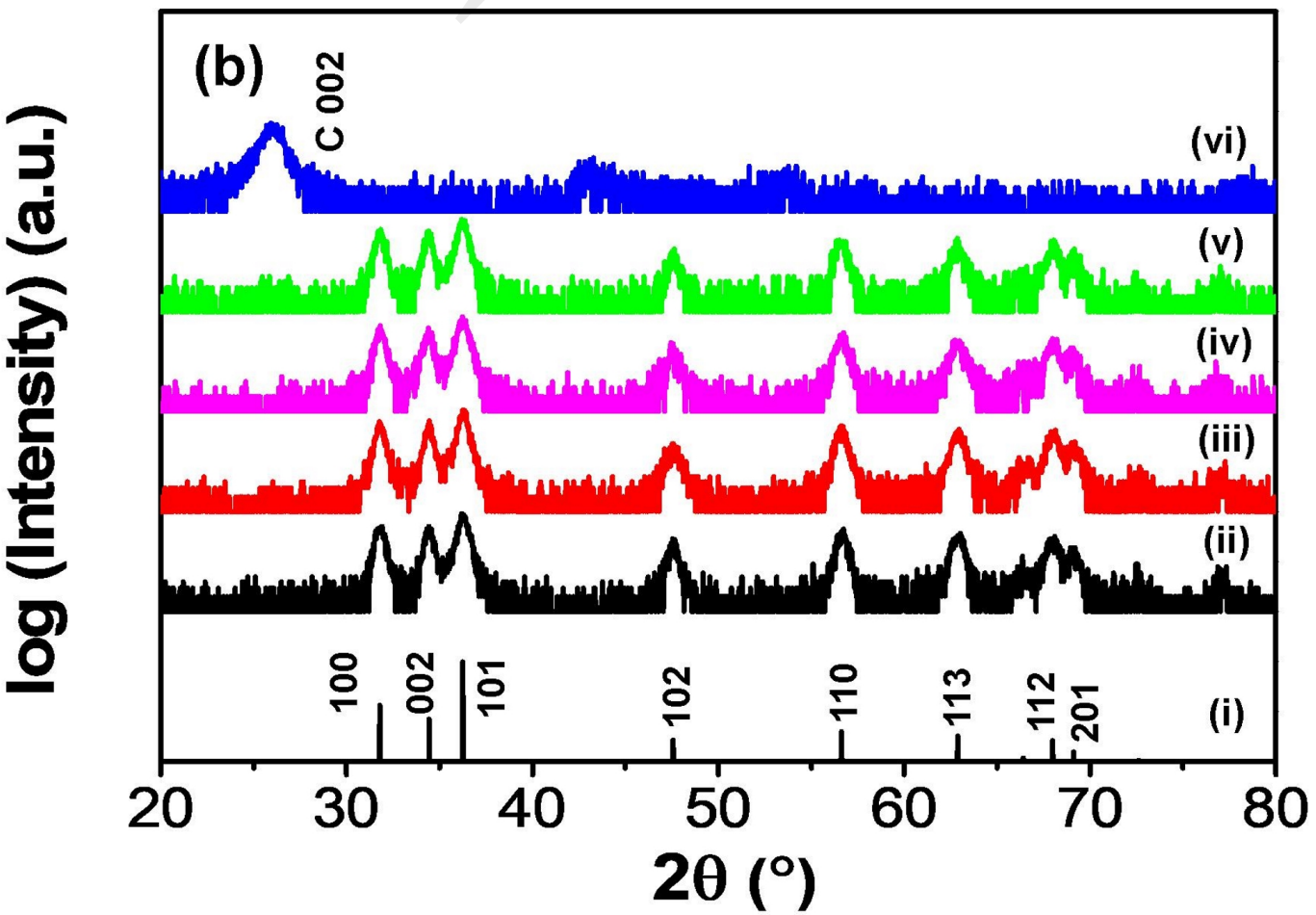
(b)
C 002
(vi)
(v)
(iv)
(iii)
(ii)
(i)
100
002
101
102
110
113
112
201
log (Intensity) (a.u.)
2θ (°)

ACCEPTED

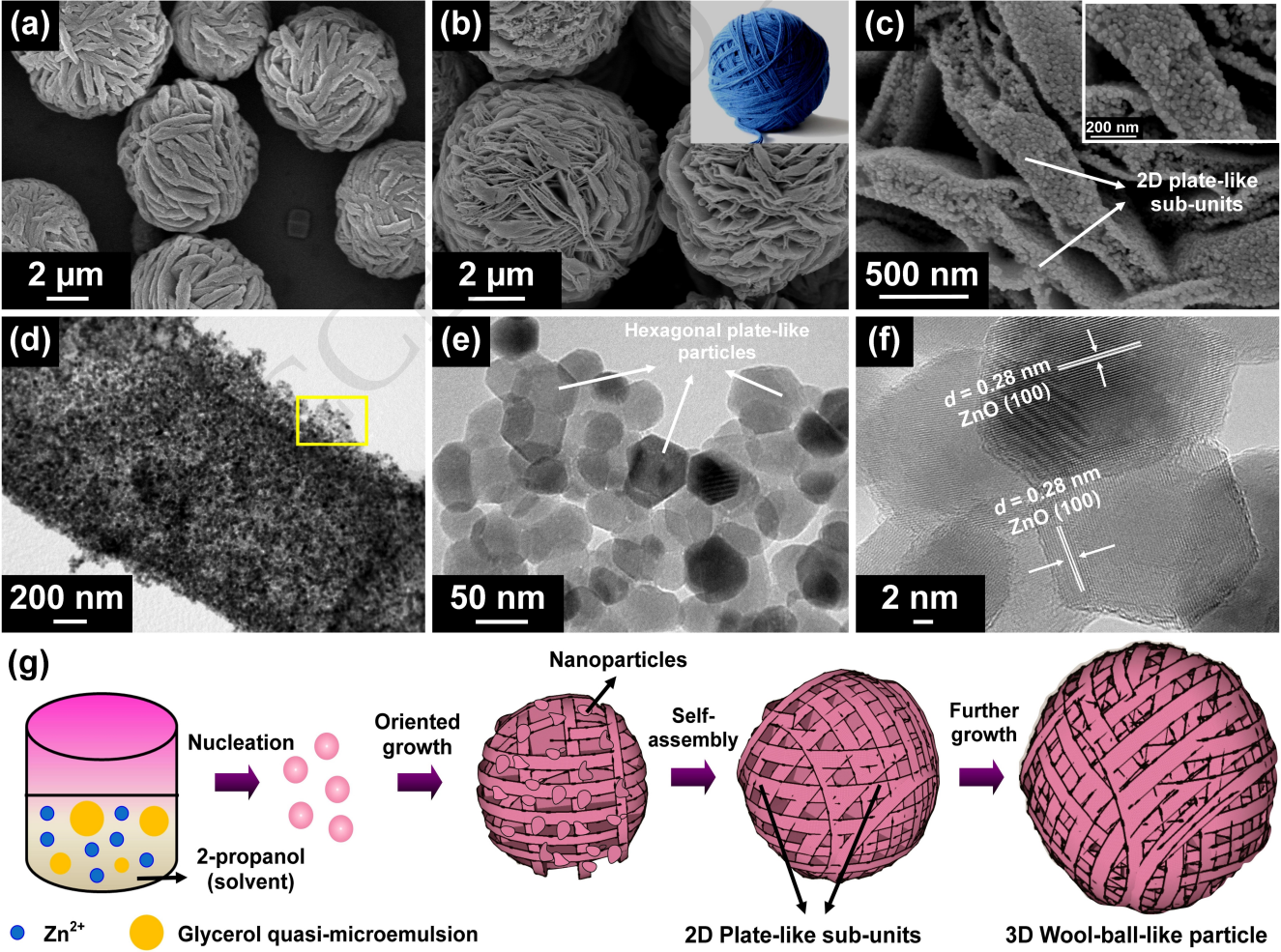
(a)
2 μm
(b)
2 μm
(c)
200 nm
2D plate-like sub-units
500 nm
(d)
200 nm
(e)
Hexagonal plate-like particles
50 nm
(f)
d = 0.28 nm ZnO (100)
d = 0.28 nm ZnO (100)
2 nm
(g)
Nucleation
2-propanol (solvent)
Oriented growth
Nanoparticles
Self-assembly
Further growth
Zn2+
Glycerol quasi-microemulsion
2D Plate-like sub-units
3D Wool-ball-like particle

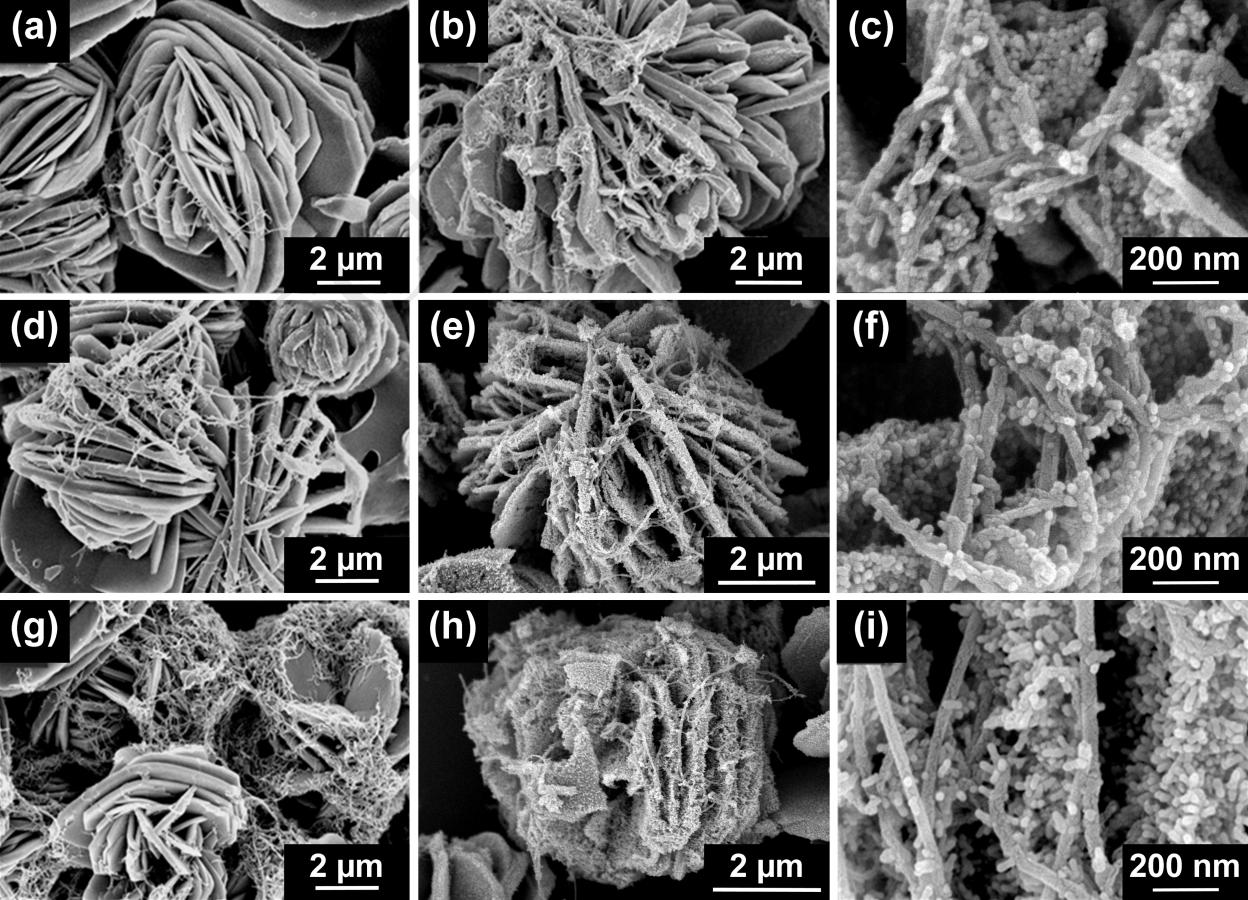
(a)
2 μm
(b)
2 μm
(c)
200 nm
(d)
2 μm
(e)
2 μm
(f)
200 nm
(g)
2 μm
(h)
2 μm
(i)
200 nm

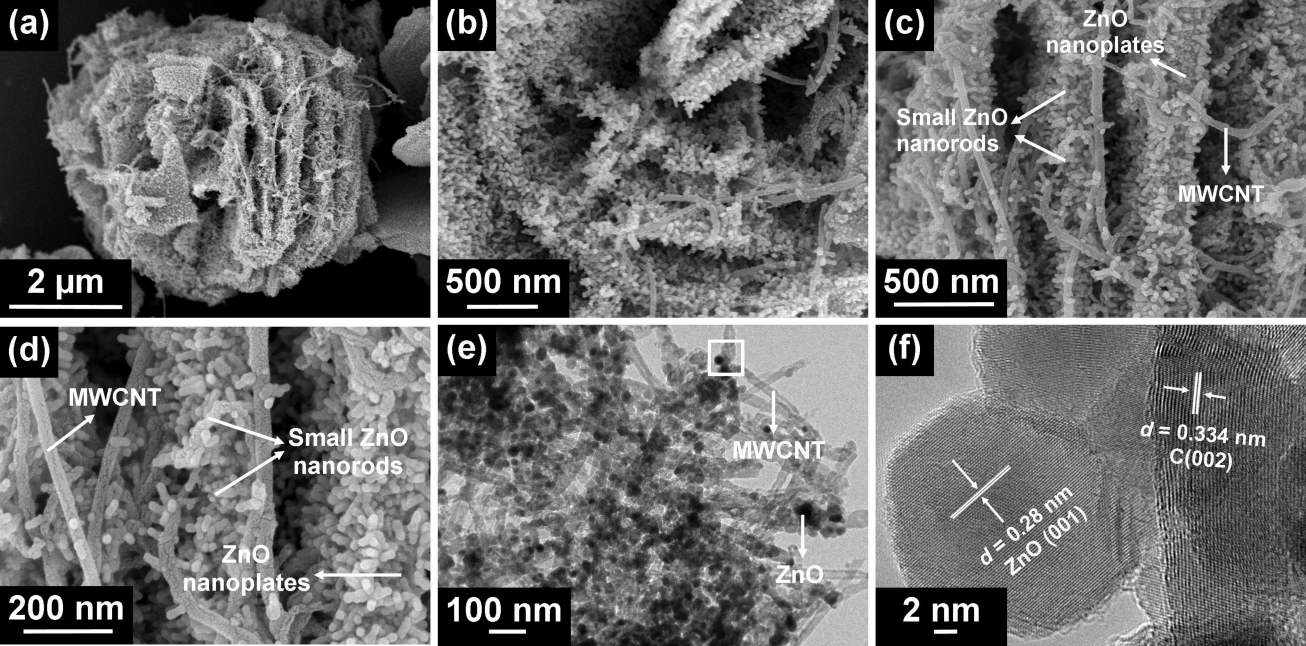
(a)
2 μm
(b)
500 nm
(c)
ZnO
nanoplates
Small ZnO
nanorods
MWCNT
500 nm
(d)
MWCNT
Small ZnO
nanorods
ZnO
nanoplates
200 nm
(e)
MWCNT
ZnO
100 nm
(f)
d = 0.334 nm
C(002)
d = 0.28 nm
ZnO (001)
2 nm

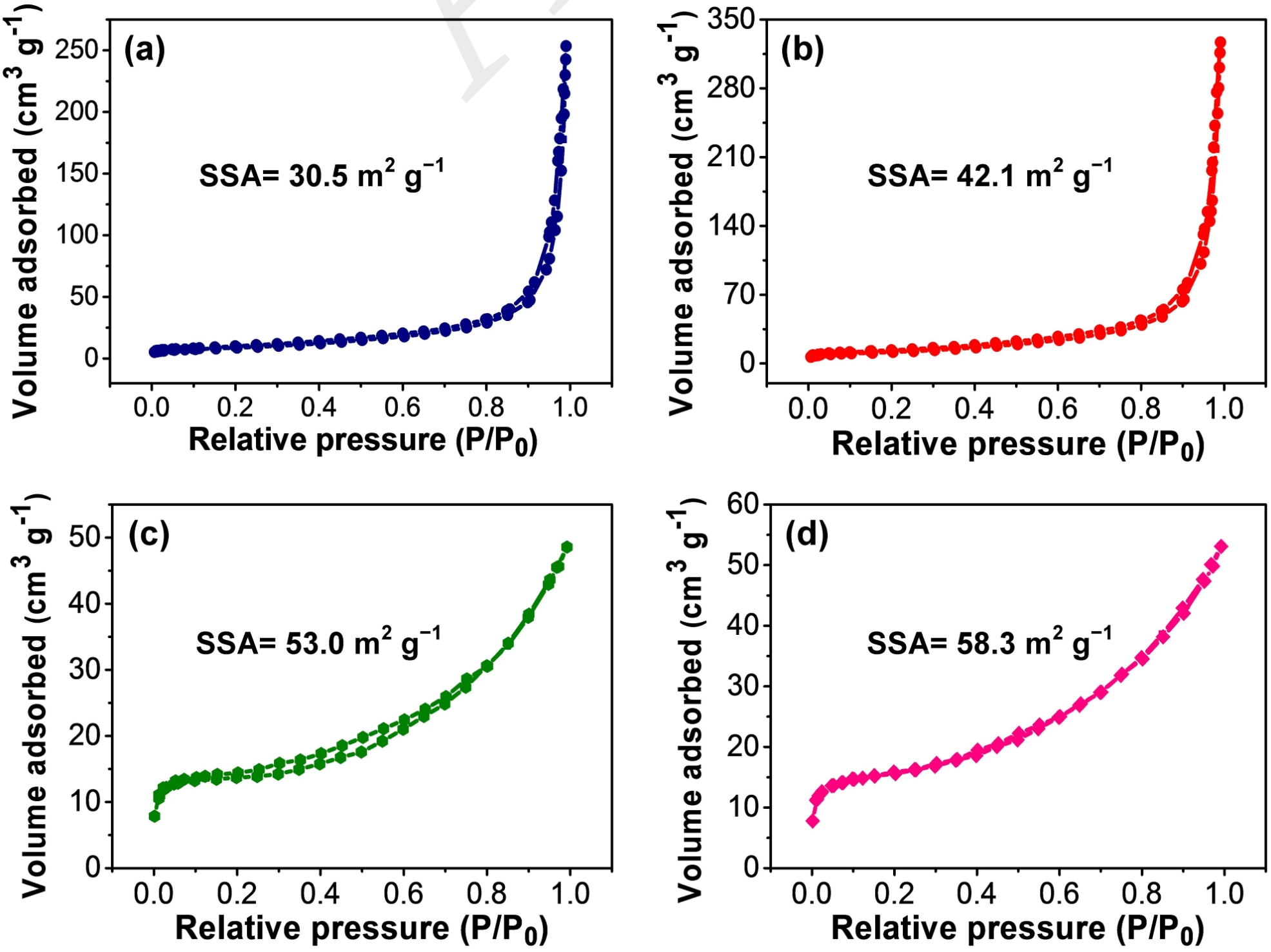
(a)
SSA= 30.5 m² g⁻¹
Volume adsorbed (cm³ g⁻¹)
Relative pressure (P/P0)
(b)
SSA= 42.1 m² g⁻¹
Volume adsorbed (cm³ g⁻¹)
Relative pressure (P/P0)
(c)
SSA= 53.0 m² g⁻¹
Volume adsorbed (cm³ g⁻¹)
Relative pressure (P/P0)
(d)
SSA= 58.3 m² g⁻¹
Volume adsorbed (cm³ g⁻¹)
Relative pressure (P/P0)

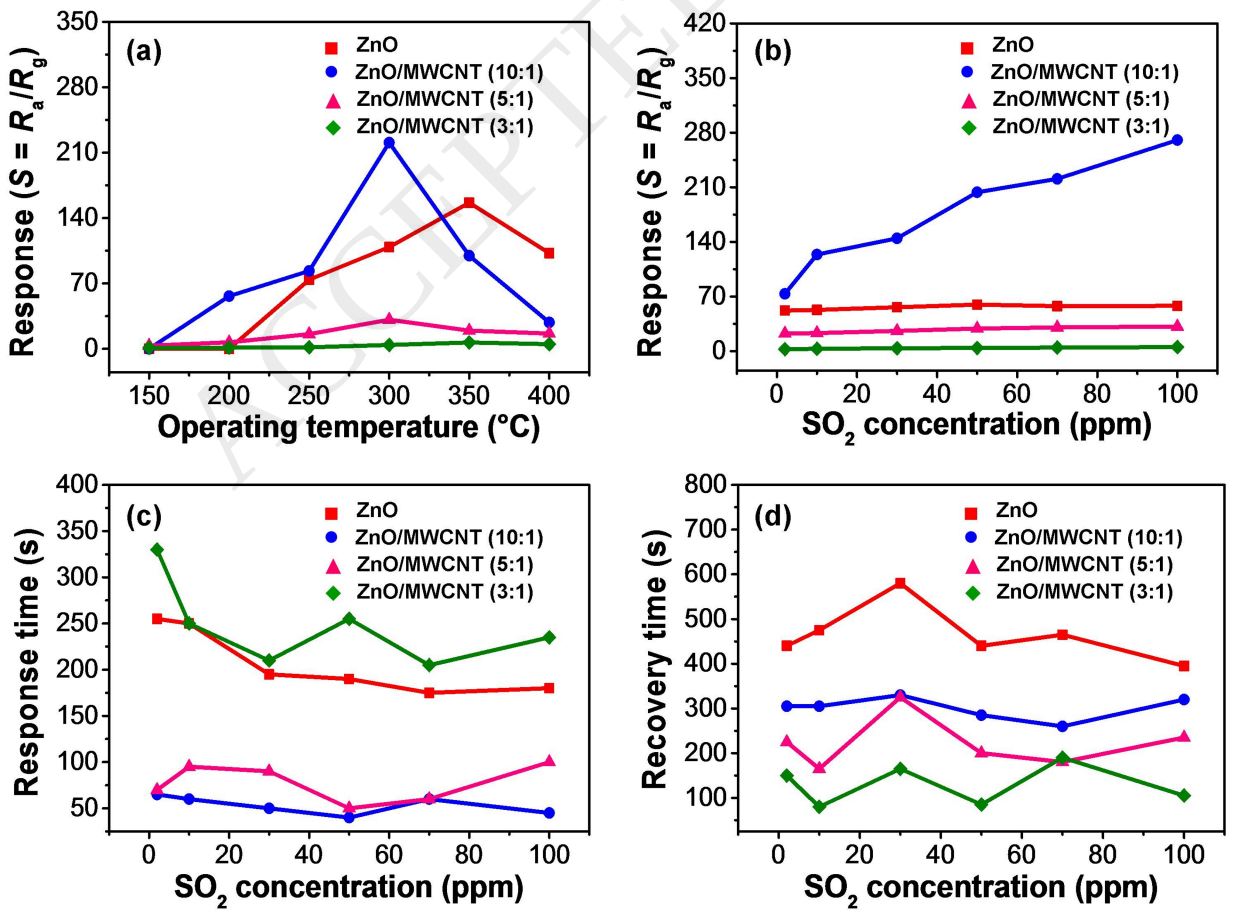
(a)
ZnO
ZnO/MWCNT (10:1)
ZnO/MWCNT (5:1)
ZnO/MWCNT (3:1)
Response ($S = R_a/R_g$)
Operating temperature (°C)
(b)
ZnO
ZnO/MWCNT (10:1)
ZnO/MWCNT (5:1)
ZnO/MWCNT (3:1)
Response ($S = R_a/R_g$)
SO_2 concentration (ppm)
(c)
ZnO
ZnO/MWCNT (10:1)
ZnO/MWCNT (5:1)
ZnO/MWCNT (3:1)
Response time (s)
SO_2 concentration (ppm)
(d)
ZnO
ZnO/MWCNT (10:1)
ZnO/MWCNT (5:1)
ZnO/MWCNT (3:1)
Recovery time (s)
SO_2 concentration (ppm)

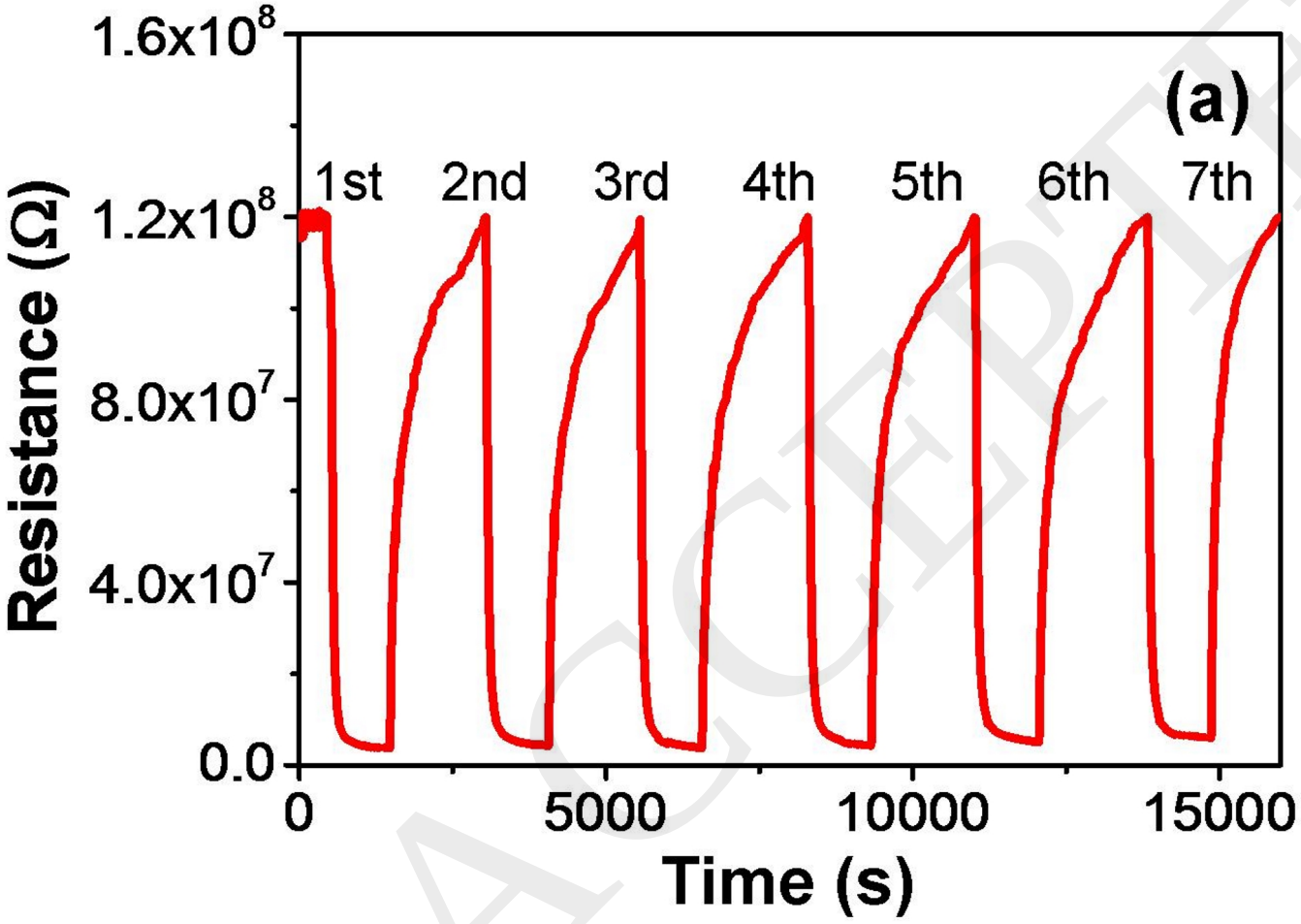
(a)
1st
2nd
3rd
4th
5th
6th
7th
Resistance (Ω)
1.6x10^8
1.2x10^8
8.0x10^7
4.0x10^7
0.0
0
5000
10000
15000
Time (s)

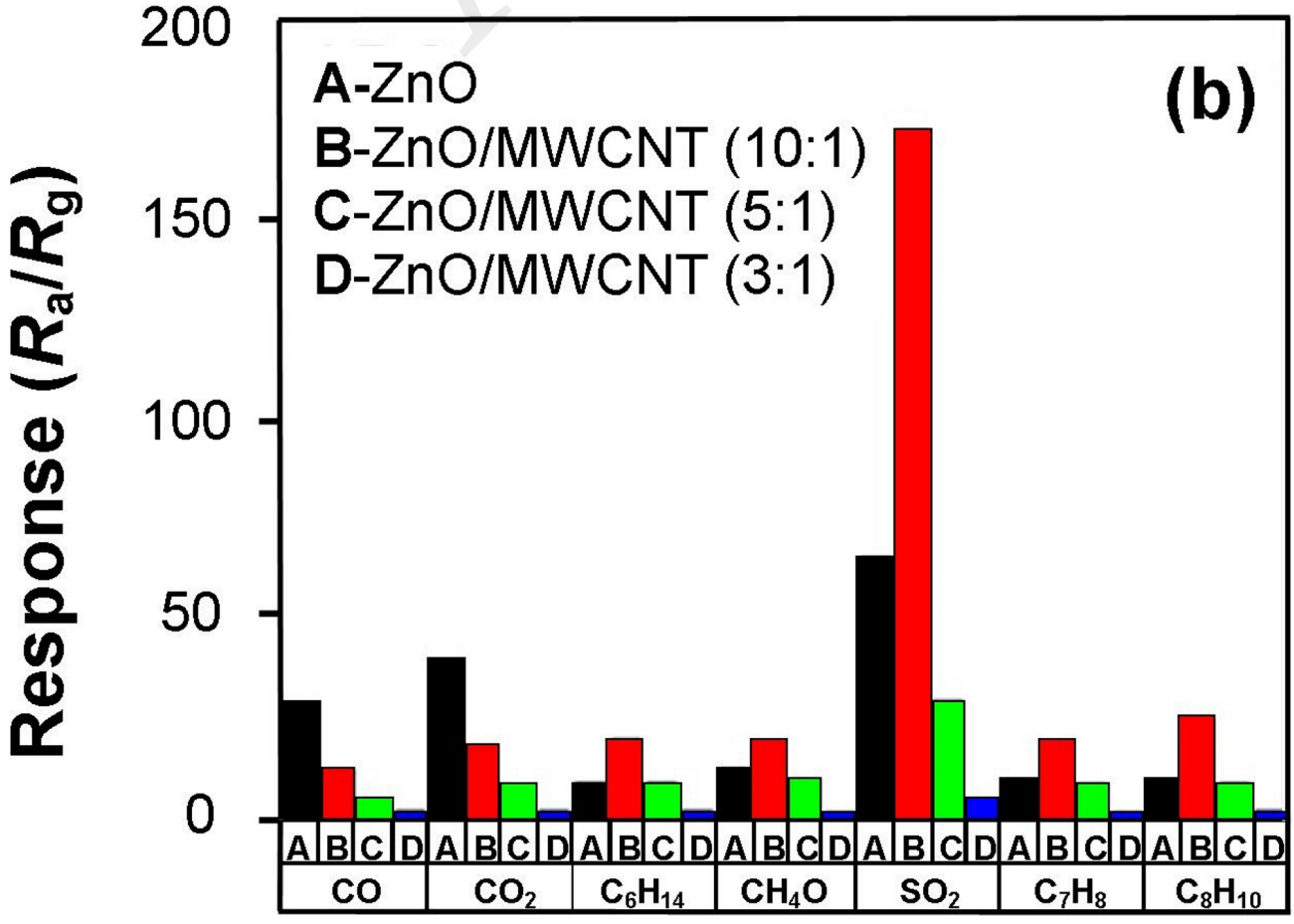
(b)
A-ZnO
B-ZnO/MWCNT (10:1)
C-ZnO/MWCNT (5:1)
D-ZnO/MWCNT (3:1)
Response (Ra/Rg)
200
150
100
50
0
A B C D A B C D A B C D A B C D A B C D A B C D A B C D
CO
CO2
C6H14
CH4O
SO2
C7H8
C8H10

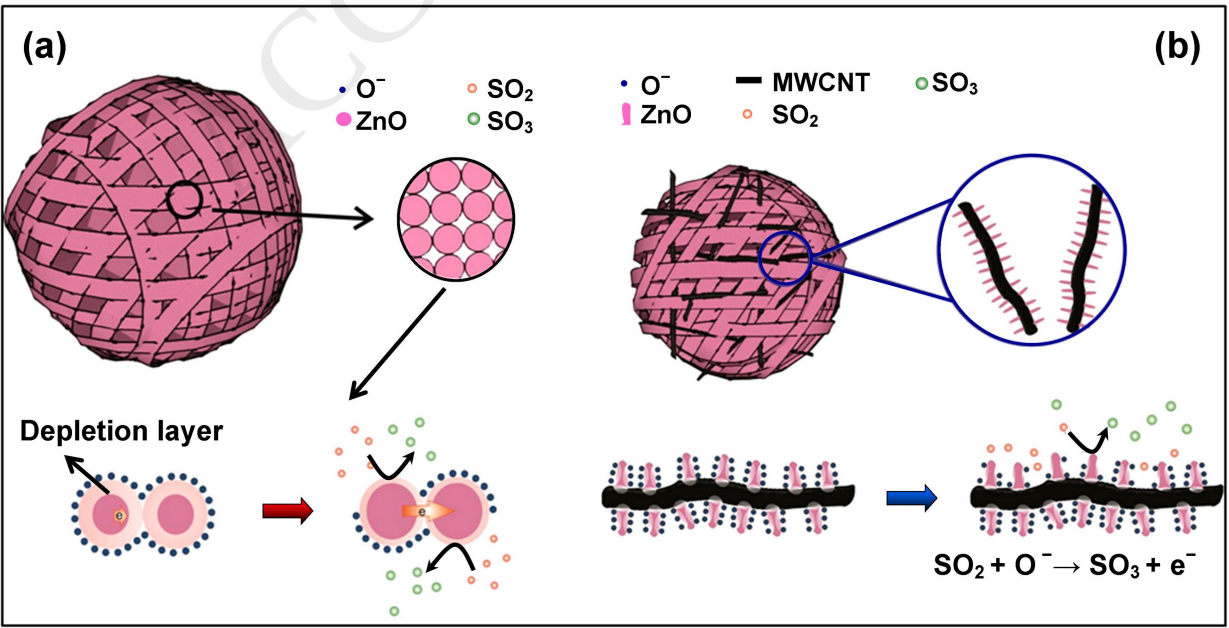
(a)
O⁻
SO2
ZnO
SO3
Depletion layer
e
e
(b)
O⁻
MWCNT
SO3
ZnO
SO2
SO2 + O⁻ → SO3 + e⁻

ACCEPTED MANUSCRIPT

LIST OF TABLES

Table 1. Comparison of the SO_2 sensing performance of the pure wool-ball-like ZnO and wool-ball-like ZnO/MWCNTs (10:1) sensors against previously reported sensors based on semiconducting metal oxide nanostructures.

Sensing material	$T_{optimum}$ **(°C)**	**Concentration (ppm)**	S **(**R_a/R_g **or** R_g/R_a**)**	**Ref.**
Wool-ball-like ZnO/MWCNTs (10:1) composite	300	70	221	This work
Wool-ball-like ZnO	350	70	151	This work
Unloaded WO_3	350	200	3.00	[52]
Unloaded WO_3	400	800	12.0	[53]
SnO_2 nanoparticles	300	500	6.00	[54]
ZnO microflowers	260	100	30.4	[64]
$CuCo_2O_4$ nanotubes	300	400	41.0	[56]
$ZnCo_2O_4$ nanotubes	300	400	2.83	[56]
$NiCo_2O_4$ nanotubes	300	400	3.78	[56]
WO_3/Ag (1.0 wt%)	450	800	21.5	[53]
Pt-loaded WO_3	200	1	5.90	[65]
SnO_2/V_2O_5 (0.15 wt%)	350	100	70.0	[55]